

# Suppression of turbulence and subcritical fluctuations in differentially rotating gyrokinetic plasmas

A A Schekochihin,<sup>1,2</sup> E G Highcock<sup>1-5</sup> and S C Cowley<sup>4,6</sup>

<sup>1</sup> Rudolf Peierls Centre for Theoretical Physics, University of Oxford, 1 Keble Rd, Oxford OX1 3NP, UK

<sup>2</sup> Merton College, Oxford OX1 4JD, UK

<sup>3</sup> Magdalen College, Oxford OX1 4AU, UK

<sup>4</sup> Euratom/CCFE Association, Culham Science Centre, Abingdon OX14 3DB, UK

<sup>5</sup> Wolfgang Pauli Institute, University of Vienna, A1090 Vienna, Austria

<sup>6</sup> Blackett Laboratory, Imperial College, London SW7 2AZ, UK

E-mail: a.schekochihin1@physics.ox.ac.uk

**Abstract.** Differential rotation is known to suppress linear instabilities in fusion plasmas. However, numerical experiments show that even in the absence of growing eigenmodes, subcritical fluctuations that grow transiently can lead to sustained turbulence, limiting the ability of the velocity shear to suppress anomalous transport. Here transient growth of electrostatic fluctuations driven by the parallel velocity gradient (PVG) and the ion temperature gradient (ITG) in the presence of a perpendicular ( $\mathbf{E} \times \mathbf{B}$ ) velocity shear is considered. The maximally simplified (but most promising for transport reduction) case of zero magnetic shear is treated in the framework of a local shearing box approximation. In this case there are no linearly growing eigenmodes, so all excitations are transient. In the PVG-dominated regime, the maximum amplification factor is found to be  $e^N$  with  $N \propto q/\epsilon$  (safety factor/aspect ratio), the maximally amplified wavenumbers perpendicular and parallel to the magnetic field are related by  $k_y \rho_i \approx (\epsilon/q)^{1/3} k_{\parallel} v_{thi}/S$ , where  $\rho_i$  is the ion Larmor radius,  $v_{thi}$  the ion thermal speed and  $S$  the  $\mathbf{E} \times \mathbf{B}$  shear. In the ITG-dominated regime,  $N$  is independent of wavenumber and  $N \propto v_{thi}/(L_T S)$ , where  $L_T$  is the ion-temperature scale length. Intermediate ITG-PVG regimes are also analysed and  $N$  is calculated as a function of  $q/\epsilon$ ,  $L_T$  and  $S$ . Analytical results are corroborated and supplemented by linear gyrokinetic numerical tests. Regimes with  $N \lesssim 1$  for all wavenumbers are possible for sufficiently low values of  $q/\epsilon$  ( $\lesssim 7$  in our model); ion-scale turbulence is expected to be fully suppressed in such regimes. For cases when it is not suppressed, an elementary heuristic theory of subcritical PVG turbulence leading to a scaling of the associated ion heat flux with  $q$ ,  $\epsilon$ ,  $S$  and  $L_T$  is proposed; it is argued that the transport is much less “stiff” than in the ITG regime.

PACS numbers: 52.30.Gz, 52.35.Qz, 52.35.Ra, 52.55.Fa

## 1. Introduction

It has long been understood that anomalous transport in tokamaks is caused by turbulence at or just above the ion Larmor scale, which is powered by drift instabilities extracting free energy from background gradients. The ion-temperature-gradient (ITG) instability [40, 15, 31] and the resulting turbulence [17] have been identified as a particular culprit. With the advent first of gyrofluid and then gyrokinetic numerical simulations, ITG turbulence has been the main focus of numerical studies aiming to map out levels of turbulent transport expected for any given set of equilibrium parameters (mean profile gradients and the magnetic configuration) [30, 18, 29, 8]. These studies assumed that the differential (toroidal) rotation of the tokamak plasmas, caused by momentum injection from the heating beams, had a negligible effect on the turbulence and on the resulting transport. This, however, is known to be an inadequate approximation for many devices and configurations in which the rotational shear can be comparable to the typical turbulent rate of strain. Linear eigenmode analysis [3, 5, 20, 14] suggests that the ITG growth rates are reduced and can be completely quenched by  $\mathbf{E} \times \mathbf{B}$  shear. A reduction or even complete suppression of associated transport was therefore expected and indeed found numerically, at least for some parameter regimes [28, 39, 9] — a result that kindled high hopes for controlling turbulence with shear and achieving transport bifurcations to steeper temperature gradients [21, 48].

Since the tokamak rotation is (to lowest order in the gyrokinetic expansion) purely toroidal [27, 16, 10, 13, 2], strong perpendicular  $\mathbf{E} \times \mathbf{B}$  shear comes at the price of a (stronger by a factor of  $q/\epsilon$ ) parallel velocity gradient (PVG) — which is itself a source of free energy and so can trigger a drift instability [11], which in turns gives rise to turbulence and anomalous transport [47, 19, 7]. This instability is in fact also suppressed by the  $\mathbf{E} \times \mathbf{B}$  shear, but only in the sense that no unstable eigenmodes survive at large enough velocity and small enough magnetic shear: transient linear amplification is still possible [45, 46, 35]. This transient amplification (illustrated in figure 1) can be sufficient to give rise to subcritically excited turbulence [7, 25, 26]. It is this turbulence that limits the effectiveness of differential rotation in suppressing anomalous transport. While transport bifurcations are still possible [25, 26, 37], finding them in the parameter space turns out to be quite a delicate task, mostly because the subcritical PVG turbulence is a largely unexplored phenomenon. In particular, it is not amenable to the usual “quasilinear” mixing-length-type arguments because those are based on the calculation of linear growth rates — and it is not obvious what should replace them for subcritical turbulence.

We take the rather obvious view that addressing this problem should start from a systematic understanding of the linear transient amplification of gyrokinetic fluctuations in the presence of velocity shear. The purest example is presented by the limit of zero (negligibly low) magnetic shear, which has the twin advantages of analytical simplicity and of being most amenable to transport bifurcations or at least

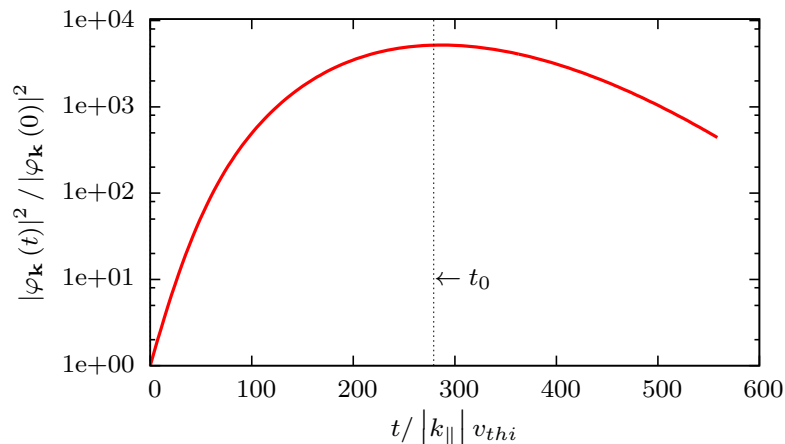


**Figure 1.** Time evolution of the squared amplitude (normalised to its initial value) of a pure-PVG-driven linear perturbation, obtained in a direct linear numerical simulation using the gyrokinetic code **AstroGK** [36] with  $1/L_n = 1/L_T = 0$ ,  $q/\epsilon = 50$ ,  $\tau/Z = 1$ ,  $k_y \rho_i = 1$ ,  $k_{\parallel} v_{thi}/S = 0.5$ . The effective growth rate for this case is shown in figure 4.

reduced levels of turbulent transport — as suggested both by numerical experiments [25, 26] and laboratory measurements [32, 33]. Formally, this regime supports no growing eigenmodes at any finite value of velocity shear, so we can focus on transient amplification and its dependence on the parameters of the problem (the ion temperature gradient, the velocity shear, the safety factor  $q$  and the device aspect ratio  $\epsilon$ ) without the complications of dealing with the transition to linear eigenmode stability. This is the kinetic treatment of this problem, following in the footsteps of the fluid theory [35] (which was done for a finite magnetic shear; note that zero magnetic shear is formally a singular limit).

Since much of the transport modeling for fusion devices relies on gyrokinetic simulations, it is important to ascertain that the linear behaviour predicted analytically is reproducible in direct gyrokinetic simulations with standard numerical codes. In what follows, we do this using the **AstroGK** code [36], which, for all practical purposes, is the slab version of the widely used fusion code **GS2**<sup>2</sup> (running **GS2** itself in slab mode produces similar results). The code solves (2) and (3) with nonlinearity switched off and a collision operator [1, 6] added to provide small-scale regularisation in phase space. These simulations demonstrate the degree to which our asymptotic results represent an adequate description of realistic parameter regimes and how the transition from the short-time to the long-time limit occurs, subject also to (minor) modifications of our results by collisions, finite resolution and numerical inaccuracies.

The rest of the paper is organised as follows. In §2, we introduce gyrokinetics in a shearing box — the governing equations of the minimal model we have chosen to treat. In §3, we consider a further simplified limit in which the ITG drive is negligible compared with the PVG drive and so we can concentrate on the essential properties of the latter, namely, work out how the transient amplification time and the amplification

<sup>2</sup> URL: <http://gyrokinetics.sourceforge.net>

exponent depend on the velocity shear,  $q$  and  $\epsilon$  and which wavenumbers prove most prone to being amplified. In § 4, we generalise these considerations by including the ITG. Both analytical and (linear) numerical results are presented throughout. A qualitative summary of the linear regime and a comparison with the fluid limit treated in [35] are given in § 5. Finally, in § 6, a criterion for the onset of subcritical PVG turbulence is proposed, followed by a very crude heuristic theory of this turbulence and of the resulting heat transport — these considerations provide a version of the standard mixing-length “quasilinear” arguments suitable for transiently growing fluctuations and a set of scaling predictions in the spirit of [8]. In particular, we give a semi-quantitative form to the argument that heat transport must be much much less “stiff” in the presence of velocity shear [32, 33, 25, 26] than in the standard ITG regime because the turbulence is no longer driven by the temperature gradient.

## 2. Gyrokinetics in a shearing box

Consider a plasma in a strong mean magnetic field. On the assumption of axisymmetry, this field can be expressed in the form  $\mathbf{B} = I(\psi)\nabla\phi + \nabla\psi \times \nabla\phi$ , where  $\psi$  (magnetic flux) and  $I(\psi)$  are two scalar functions determined by solving the mean MHD equilibrium equations and  $\phi$  is the azimuthal angle with respect to which symmetry is assumed. It can be shown (see [2] and references therein) that if such a plasma rotates with some velocity ordered in the gyrokinetic expansion as similar in size to the speed of sound, this mean rotation must be purely azimuthal, the same for both species and with an angular velocity  $\omega$  that depends on the flux label  $\psi$  only:  $\mathbf{u} = \omega(\psi)R^2\nabla\phi$ , where  $R$  is the radial coordinate. Thus, each of the nested toroidal flux surfaces rotates at its own rate and there is a velocity shear set up by the variation of  $\omega$  with  $\psi$ . In this paper, we will be concerned only with the effect on the plasma stability of this differential character of the rotation. Formally, this effect is isolated by assuming the Mach number  $M = u/v_{\text{thi}}$  ( $v_{\text{thi}}$  is the ion thermal speed) to be moderately low. Mathematically, this can be cast as an expansion in  $M \ll 1$  (subsidiary to the gyrokinetic expansion) where, while the mean velocity is ordered subsonic,  $u \sim O(M)$ , its scale length is ordered as  $O(1/M)$ . Under this scheme, effects such the Coriolis or centrifugal motion (as well as other, more obscure, ones) that scale with the magnitude of the mean velocity are negligible, while velocity gradients are retained.

Let us consider the vicinity of some flux surface  $\psi = \psi_0$  and introduce a local orthogonal Cartesian frame  $(x, y, z)$  that is moving with the flux surface  $\psi_0$  and in which  $x$  is the cross-flux-surface (“radial”) coordinate,  $z$  is the coordinate in the direction of the magnetic field and  $y$  completes the orthogonal frame ( $\hat{\mathbf{y}} = \hat{\mathbf{z}} \times \hat{\mathbf{x}}$ ). Then the velocity field can be replaced by a pure linear shear flow:

$$\mathbf{u} \cdot \nabla \approx Sx \frac{\partial}{\partial y}, \quad S = \frac{B_p^2 R^2}{B} \frac{d\omega}{d\psi}, \quad (1)$$

where  $B_p = |\nabla\psi|/R$  is the poloidal magnetic field (see Appendix A.1 for details; figure 2 illustrates the geometry). This model might be called the “flying slab approximation,”

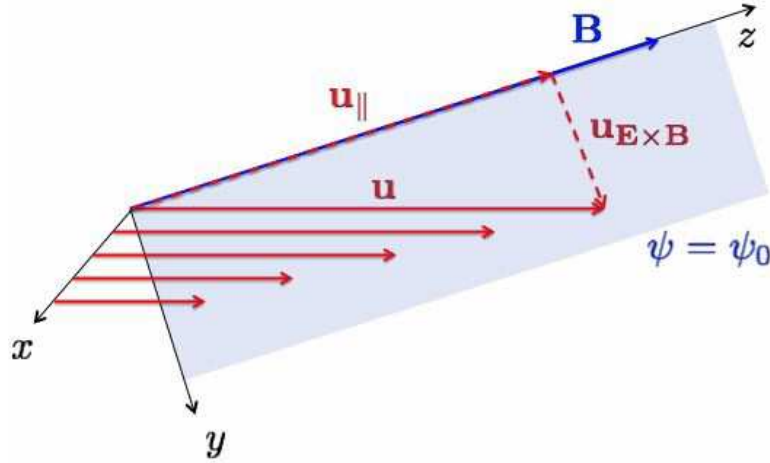


**Figure 2.** Magnetic field, velocity field (sheared) and the local Cartesian frame. The reference flux surface  $\psi = \psi_0$  is shaded.

or, perhaps more conventionally, the shearing box — a common analytical simplification in the fluid dynamics of differentially rotating systems [23].

We will make three further simplifying approximations by assuming all fluctuations to be electrostatic, electrons to have purely Boltzmann response and the mean magnetic field to be (locally) straight and uniform, so it has neither curvature nor variation of magnitude nor shear (which means that the magnetic drifts can be dropped). With all these assumptions and working in the flying slab (shearing box), we can write the gyrokinetic system of equations in the following form (see Appendix A)

$$\begin{aligned} \frac{\partial h}{\partial t} + Sx \frac{\partial h}{\partial y} + w_{\parallel} \frac{\partial h}{\partial z} + \frac{\rho_i v_{\text{th}i}}{2} \left( \frac{\partial \langle \tilde{\varphi} \rangle_{\mathbf{R}}}{\partial x} \frac{\partial h}{\partial y} - \frac{\partial \langle \tilde{\varphi} \rangle_{\mathbf{R}}}{\partial y} \frac{\partial h}{\partial x} \right) &= \left( \frac{\partial}{\partial t} + Sx \frac{\partial}{\partial y} \right) \langle \tilde{\varphi} \rangle_{\mathbf{R}} \\ - \frac{\rho_i v_{\text{th}i}}{2} \frac{\partial \langle \tilde{\varphi} \rangle_{\mathbf{R}}}{\partial y} \left[ \frac{1}{L_n} + \left( \frac{w^2}{v_{\text{th}i}^2} - \frac{3}{2} \right) \frac{1}{L_T} - \frac{2w_{\parallel} q}{v_{\text{th}i}^2 \epsilon} S \right] F_0, \end{aligned} \quad (2)$$

$$\left( 1 + \frac{\tau}{Z} \right) \tilde{\varphi} = \frac{1}{n_i} \int d^3 \mathbf{w} \langle h \rangle_{\mathbf{r}}, \quad (3)$$

where  $h(t, \mathbf{R}, w, w_{\parallel})$  is the ion gyrocentre distribution function,  $F_0(\psi, w)$  the equilibrium Maxwellian (of the ions),  $\tilde{\varphi}(t, \mathbf{r}) = Ze\varphi/T_i$  the nondimensionalised electrostatic potential ( $Ze$  is the ion charge),  $\rho_i$  the ion Larmor radius,  $n_i$  the ion number density,  $\mathbf{w}$  the particles' peculiar velocity with respect to the mean flow,  $\mathbf{r}$  the position coordinate,  $\mathbf{R}$  the guiding-centre coordinate, and the angle brackets denote the gyroaverages holding constant the coordinate appearing in their subscript (the precise definitions are provided in Appendix A). We have defined the equilibrium gradients and two other standard parameters as follows

$$\frac{1}{L_n} = -B_p R \frac{d \ln n_i}{d\psi}, \quad \frac{1}{L_T} = -B_p R \frac{d \ln T_i}{d\psi}, \quad \frac{q}{\epsilon} = \frac{B_{\phi}}{B_p}, \quad \tau = \frac{T_i}{T_e}, \quad (4)$$

where  $n_i$  and  $T_i$  are the ion density and temperature, respectively, and  $B_{\phi}$  is the azimuthal mean magnetic field.

Note that the velocity shear  $S$  appears in two ways in (2): as perpendicular shear (multiplying  $x \partial/\partial y$ ) and as parallel shear (multiplying  $F_0$  in the right-hand side). The perpendicular shear rips apart the unstable fluctuations and will have a stabilising effect, whereas the parallel shear (the PVG) acts as a source of free energy in a manner analogous to ITG and drives a drift instability (§3.1). The relative size of these two effects is set by the value of  $q/\epsilon$ .

### 2.1. Case of non-zero magnetic shear

Including a (locally) constant linear magnetic shear into the problem amounts to replacing in (2)

$$Sx \frac{\partial h}{\partial y} \rightarrow \left( S + \frac{w_{\parallel}}{L_s} \right) x \frac{\partial h}{\partial y}, \quad (5)$$

where  $L_s$  is the scale length associated with the magnetic shear. This appears to introduce complications as we now have an “effective shear” that depends on the particle velocity  $w_{\parallel}$ . However, since the size of  $w_{\parallel}$  is constrained by the Maxwellian equilibrium distribution, this term can be neglected provided  $M_s = SL_s/v_{\text{thi}} \gg 1$ . Under this assumption, the theory developed below applies without modification. We note that the “shear Mach number”  $M_s$  is precisely the parameter that is known to control linear stability and transient amplification of in the ITG-PVG-driven plasmas in the fluid (collisional) limit [35].

### 2.2. Shearing frame

The next step — standard in treatments of systems with linear shear — is to make a variable transformation  $(t, \mathbf{r}) \rightarrow (t', \mathbf{r}')$  that removes the shear terms ( $Sx \partial/\partial y$ ):

$$t' = t, \quad x' = x, \quad y' = y - Sxt, \quad z' = z, \quad (6)$$

and similarly for  $(t, \mathbf{R}) \rightarrow (t', \mathbf{R}')$ . The Fourier transform can then be performed in the primed variables, so

$$\tilde{\varphi} = \sum_{\mathbf{k}'} \tilde{\varphi}_{\mathbf{k}'}(t') e^{i\mathbf{k}' \cdot \mathbf{r}'} = \sum_{\mathbf{k}'} \tilde{\varphi}_{\mathbf{k}'}(t') e^{i\mathbf{k}(\mathbf{k}', t') \cdot \mathbf{r}}, \quad (7)$$

where  $k_x = k'_x - Sk'_y t'$ ,  $k_y = k'_y$ , and  $k_{\parallel} = k'_{\parallel}$  (we denote  $k_{\parallel} \equiv k_z$ ). As usual in the gyrokinetic theory, working in Fourier space allows us to compute the gyroaverages in terms of Bessel functions:

$$\langle \tilde{\varphi} \rangle_{\mathbf{R}} = \sum_{\mathbf{k}'} J_0(a(t')) \tilde{\varphi}_{\mathbf{k}'}(t') e^{i\mathbf{k}' \cdot \mathbf{R}'}, \quad \langle h \rangle_{\mathbf{r}} = \sum_{\mathbf{k}'} J_0(a(t')) h_{\mathbf{k}'}(t') e^{i\mathbf{k}' \cdot \mathbf{r}'}, \quad (8)$$

where  $a(t') = k_{\perp} w_{\perp} / \Omega_i = (w_{\perp} / \Omega_i) \sqrt{(k'_x - Sk'_y t')^2 + k'^2_y} = (k'_y w_{\perp} / \Omega_i) \sqrt{1 + S^2 t'^2}$ , and we have shifted the origin of time:  $t'' = t' - S^{-1} k'_x / k'_y$ .

Finally, we rewrite the gyrokinetic system (2)–(3) in the new variables  $(t'', \mathbf{k}')$ . Since we are interested only in the linear problem here, we will drop the nonlinearity. We also

suppress all primes in the variables. The result is

$$\frac{\partial h_{\mathbf{k}}}{\partial t} + ik_{\parallel} w_{\parallel} h_{\mathbf{k}} = \left\{ \frac{\partial}{\partial t} - i \left[ \omega_* + \left( \frac{w^2}{v_{\text{thi}}^2} - \frac{3}{2} \right) \omega_* \eta_i - \frac{w_{\parallel}}{v_{\text{thi}}} \frac{q}{\epsilon} S k_y \rho_i \right] \right\} F_0 J_0(a(t)) \tilde{\varphi}_{\mathbf{k}}, \quad (9)$$

$$\left( 1 + \frac{\tau}{Z} \right) \tilde{\varphi}_{\mathbf{k}} = \frac{1}{n} \int d^3 \mathbf{w} J_0(a(t)) h_{\mathbf{k}}, \quad (10)$$

where  $\omega_* = k_y \rho_i v_{\text{thi}} / 2L_n$  is the drift frequency and  $\eta_i = L_n / L_T$ ; the argument of the Bessel function is  $a(t) = (w_{\perp} / v_{\text{thi}}) k_y \rho_i \sqrt{1 + S^2 t^2}$ .

### 2.3. Integral equation for the linearised problem

We integrate (9) with respect to time, assume the initial fluctuation amplitude small compared to values to which it will grow during the subsequent time evolution, rescale time  $|k_{\parallel}| v_{\text{thi}} t \rightarrow t$ , denote  $\Delta t = t - t'$ , use (10), in which the velocity integrals involving the Maxwellian  $F_0 = n e^{-w^2/v_{\text{thi}}^2} / (\pi v_{\text{thi}}^2)^{3/2}$  are done in the usual way, and obtain finally the following integral equation for  $\tilde{\varphi}(t)$ :

$$\left( 1 + \frac{\tau}{Z} - \Gamma_0(\lambda, \lambda) \right) \tilde{\varphi}(t) = \int_0^t d\Delta t e^{-\Delta t^2/4} \left\{ \left( \frac{q}{\epsilon} \bar{\omega}_S - 1 \right) \frac{\Delta t}{2} - i \bar{\omega}_* \left[ 1 + \eta_i \left( \Lambda(\lambda, \lambda') - 1 - \frac{\Delta t^2}{4} \right) \right] \right\} \Gamma_0(\lambda, \lambda') \tilde{\varphi}(t - \Delta t), \quad (11)$$

where  $\bar{\omega}_* = \omega_* / |k_{\parallel}| v_{\text{thi}} = k_y \rho_i / 2 |k_{\parallel}| L_n$  is the normalised drift frequency,  $\bar{\omega}_S = S k_y \rho_i / k_{\parallel} v_{\text{thi}}$  the normalised shear parameter, and

$$\Gamma_0(\lambda, \lambda') = e^{-(\lambda + \lambda')/2} I_0(\sqrt{\lambda \lambda'}), \quad \Lambda(\lambda, \lambda') = 1 - \frac{\lambda + \lambda'}{2} + \sqrt{\lambda \lambda'} \frac{I_1(\sqrt{\lambda \lambda'})}{I_0(\sqrt{\lambda \lambda'})}, \quad (12)$$

where  $\lambda(t) = (k_y^2 \rho_i^2 + \bar{\omega}_S^2 t^2) / 2$ ,  $\lambda' = \lambda(t') = (k_y^2 \rho_i^2 + \bar{\omega}_S^2 t'^2) / 2$ , and  $I_0$  and  $I_1$  are modified Bessel functions of the first kind.

Equation (11) is the master equation for the linear time evolution of the plasma fluctuations driven by the ITG (the  $\bar{\omega}_* \eta_i$  term) and the PVG (the  $(q/\epsilon) \bar{\omega}_S$  term).

### 3. Solution for the case of strong shear

We will first consider the maximally simplified case of pure PVG drive (strong shear). This is a good quantitative approximation to the general case if  $\bar{\omega}_*, \eta_i \bar{\omega}_* \ll (q/\epsilon) \bar{\omega}_S$ , which in terms of the basic dimensional parameters of the problem translates into

$$\frac{qS}{\epsilon} \gg \frac{v_{\text{thi}}}{L_n}, \frac{v_{\text{thi}}}{L_T}. \quad (13)$$

This is the regime into which the plasma is pushed as the flow shear is increased — under certain conditions, the transition can occur abruptly, via a transport bifurcation [25, 37, 26]. Besides being, therefore, physically the most interesting, this limit also has the advantage of particular analytical transparency (the more general case including ITG will be considered in §4).

Thus, neglecting all terms that contain  $\bar{\omega}_*$  and  $\eta_i$ , (11) becomes

$$\left(1 + \frac{\tau}{Z} - \Gamma_0(\lambda, \lambda)\right) \tilde{\varphi}(t) = \frac{1}{2} \int_0^t d\Delta t \Delta t e^{-\Delta t^2/4} \left(\frac{q}{\epsilon} \bar{\omega}_S - 1\right) \Gamma_0(\lambda, \lambda') \tilde{\varphi}(t - \Delta t). \quad (14)$$

### 3.1. Short-time limit: the PVG instability

Let us first consider the case in which the velocity shear is unimportant except for the PVG drive, i.e., we can approximate  $\lambda \approx \lambda' \approx k_y^2 \rho_i^2 / 2$  and so there is no time dependence in the Bessel functions in (14). We would also like to be able to assume  $t \gg 1$  so that the time integration in (14) can be extended to  $\infty$ . Formally this limiting case is achieved by ordering  $k_y \rho_i \sim 1$  and  $1 \ll t \ll 1/\bar{\omega}_S \lesssim q/\epsilon$  (in dimensional terms, this is equivalent to  $St \ll 1$ ,  $k_{\parallel} v_{thi} t \gg 1$  and  $1 \ll k_{\parallel} v_{thi} / S \lesssim q/\epsilon$ ). Physically, this regime is realised in the initial stage of evolution of the fluctuations or, equivalently, in the case of very weak shear but large  $q/\epsilon$ .

Under this ordering, we can seek solutions to (14) in the form  $\tilde{\varphi}(t) = \tilde{\varphi}_0 \exp(-i\bar{\omega}t)$ , where  $\bar{\omega} = \omega / |k_{\parallel} v_{thi}|$  is the nondimensionalised complex frequency and  $\omega$  its dimensional counterpart. The time integral in (14) can be expressed in terms of the plasma dispersion function, which satisfies [22]

$$\mathcal{Z}(\bar{\omega}) = i \int_0^{\infty} d\Delta t e^{i\bar{\omega}\Delta t - \Delta t^2/4}, \quad \mathcal{Z}'(\bar{\omega}) = -2[1 + \bar{\omega}\mathcal{Z}(\bar{\omega})]. \quad (15)$$

With the aid of these formulae, (11) is readily converted into a transcendental equation for  $\bar{\omega}$ :

$$\frac{1 + \tau/Z}{\Gamma_0(\lambda)} - 1 = \left(\frac{q}{\epsilon} \bar{\omega}_S - 1\right) [1 + \bar{\omega}\mathcal{Z}(\bar{\omega})], \quad (16)$$

where  $\Gamma_0(\lambda) = e^{-\lambda} I_0(\lambda)$ ,  $\lambda = k_y^2 \rho_i^2 / 2$  and  $\bar{\omega}_S = S k_y \rho_i / k_{\parallel} v_{thi}$ .

Equation (16) is simply the dispersion relation for the ion acoustic wave modified by the PVG drive term. This point is probably best illustrated by considering the cold-ion/long-wavelength limit  $\tau \ll 1$ ,  $\bar{\omega} = \omega / |k_{\parallel} v_{thi}| \gg 1$ ,  $\lambda = k_y^2 \rho_i^2 / 2 \ll 1$ . Then  $\Gamma_0(\lambda) \approx 1$ ,  $1 + \bar{\omega}\mathcal{Z}(\bar{\omega}) \approx -1/2\bar{\omega}^2 + i\bar{\omega}\sqrt{\pi}e^{-\bar{\omega}^2}$ , and so, restoring dimensions in (16), we get

$$\bar{\omega}^2 \approx \frac{Z}{2\tau} \left(1 - \frac{q}{\epsilon} \bar{\omega}_S\right) \Rightarrow \omega \approx \pm k_{\parallel} c_s \left(1 - \frac{qS}{\epsilon} \frac{k_y \rho_i}{k_{\parallel} v_{thi}}\right)^{1/2}, \quad (17)$$

where in the last expression, we have restored dimensions and denoted  $c_s = (Z/2\tau)^{1/2} v_{thi} = (T_e/m_i)^{1/2}$ , the sound speed. When  $(q/\epsilon)\bar{\omega}_S$  is sufficiently large, the sound wave is destabilised and turns into the PVG instability. Note that it loses its real frequency in this transition.

Some further (elementary) analytical considerations of the PVG instability are relegated to Appendix B.1. Here it will suffice to notice that if the (dimensional) growth rate  $\gamma = \text{Im} \omega$  is scaled by  $qS/\epsilon$  and  $k_{\parallel}$  by  $(qS/\epsilon)/v_{thi}$ , their mutual dependence is universal for all values of the velocity shear or  $q/\epsilon$ , namely,

$$\gamma = \frac{qS}{\epsilon} f\left(k_y \rho_i, \frac{k_{\parallel} v_{thi}}{qS/\epsilon}\right). \quad (18)$$



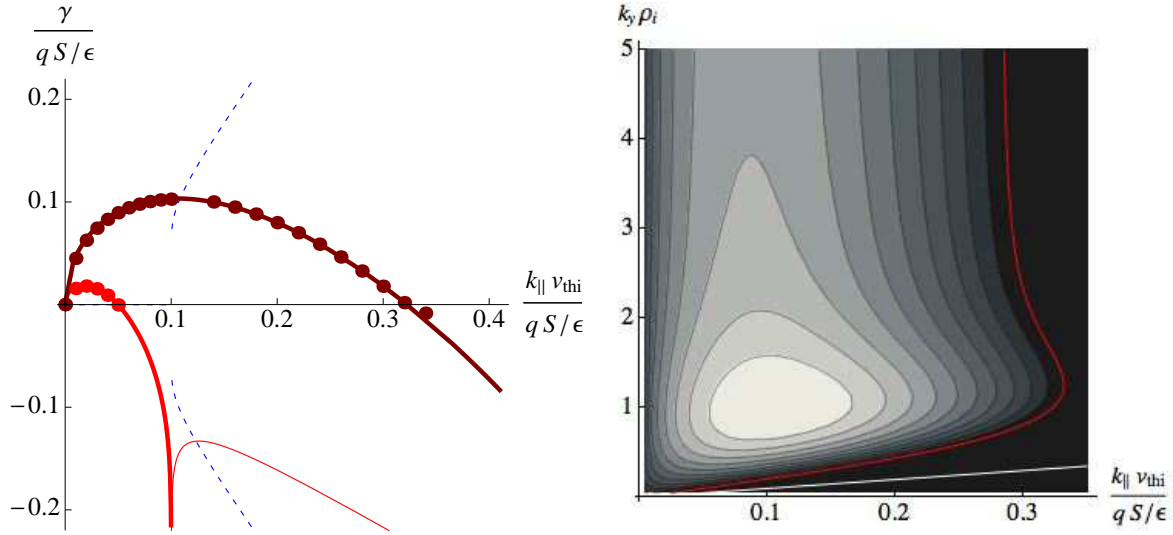


**Figure 3.** *Left panel:* Growth rate  $\gamma = \text{Im } \omega$  (normalised by  $qS/\epsilon$ ) vs.  $k_{\parallel} v_{thi}/(qS/\epsilon)$ . Here  $\tau/Z = 1$ , and the two curves are for  $k_y \rho_i = 0.1$  (red) and  $k_y \rho_i = 1$  (brown). The growth rate becomes independent of  $k_y$  for  $k_y \rho_i \gg 1$  (see end of Appendix B.1) and all curves for large  $k_y \rho_i$  are very close to each other and similar in shape to  $k_y \rho_i = 1$  (see right panel). The mode has no real frequency for  $k_{\parallel} v_{thi}/(qS/\epsilon) < k_y \rho_i$ ; for  $k_{\parallel} v_{thi}/(qS/\epsilon) > k_y \rho_i$ , it turns into a damped sound wave: the corresponding frequencies and the damping rate are shown only for  $k_y \rho_i = 0.1$ , as thin blue (dashed) and red (solid) lines, respectively. The discrete points show growth rates calculated by direct linear numerical simulation using the gyrokinetic code **AstroGK** [36]. *Right panel:* Contour plot of  $\gamma/(qS/\epsilon)$  vs.  $k_{\parallel} v_{thi}/(qS/\epsilon)$  and  $k_y \rho_i$ . Only positive values are plotted, black means  $\gamma < 0$ . The red curve shows the stability boundary (B.1). The white line shows the boundary (B.2) between PVG modes (above it) and sound waves (below it).

Once this rescaling is done, the dispersion relation (16) no longer contains any parameters (except  $\tau/Z$ , which we can safely take to be order unity). The growth rate, obtained via numerical solution of (16) with  $\tau/Z = 1$ , is plotted in figure 3. The maximum growth rate is  $\gamma_{\max} \approx 0.10(qS/\epsilon)$ . This peak value is reached when  $k_y \rho_i \approx 1.0$  and  $k_{\parallel} \approx 0.10(qS/\epsilon)/v_{thi}$ , i.e., at  $(q/\epsilon)\bar{\omega}_S \approx 10$ .

The conclusion is that, at least in the initial stage of their evolution, plasma fluctuations in a significant part of the wavenumber space ( $k_y$  and  $k_{\parallel}$  are constrained by (B.1)) are amplified by the PVG. This amplification does not, however, go on for a long time as the approximation we adopted to derive the dispersion relation (16) breaks down when  $\bar{\omega}_S t \sim k_y \rho_i$  (or  $St \sim 1$  if the dimensional units of time are restored) — this gives  $\gamma t \sim 0.1(q/\epsilon)$ , so, realistically, after barely one exponentiation. The key question is what happens after that. We will see shortly that all modes will eventually decay and that the fastest initially growing modes are in fact not quite the ones that will grow the longest or get maximally amplified.

### 3.2. Long-time limit: transient growth

Let us now investigate the long-time limit,  $\bar{\omega}_S t \gg 1$ ,  $k_y \rho_i$  (or, in dimensional form,  $St \gg 1$ ,  $k_y \rho_i St \gg 1$ ). In this limit, the kernel involving the Bessel function in (14) simplifies considerably: we have  $\lambda \approx \bar{\omega}_S^2 t^2 / 2 \gg 1$ ,  $\lambda' \approx \bar{\omega}_S^2 (t - \Delta t)^2 / 2 \gg 1$  and so

$$\Gamma_0(\lambda, \lambda') \approx \frac{e^{-(\sqrt{\lambda} - \sqrt{\lambda'})^2 / 2}}{\sqrt{2\pi\sqrt{\lambda\lambda'}}} \approx \frac{e^{-\bar{\omega}_S^2 \Delta t^2 / 4}}{\sqrt{\pi} |\bar{\omega}_S| t}. \quad (19)$$

Working to the lowest nontrivial order in  $1/t$ , we can now rewrite (14) as follows

$$\left(1 + \frac{\tau}{Z}\right) |\bar{\omega}_S| t \tilde{\varphi}(t) = \frac{1}{2\sqrt{\pi}} \int_0^\infty d\Delta t \Delta t e^{-(\bar{\omega}_S^2 + 1)\Delta t^2 / 4} \left(\frac{q}{\epsilon} \bar{\omega}_S - 1\right) \tilde{\varphi}(t - \Delta t). \quad (20)$$

We will seek a solution to this equation in the form

$$\tilde{\varphi}(t) = \tilde{\varphi}_0 \exp \left[ \int_0^t dt' \bar{\gamma}(t') \right], \quad (21)$$

where  $\bar{\gamma}(t) = \gamma(t)/|k_\parallel|v_{\text{th}i}$  is the effective time-dependent growth rate (nondimensionalised) and  $\gamma(t)$  the dimensional version of it (remember that time is scaled by  $|k_\parallel|v_{\text{th}i}$ ). Because of the exponential in the kernel, the memory of the time-history integral in the right-hand side of (20) is limited, so  $\Delta t \ll t$  and we will be able to make progress by expanding

$$\tilde{\varphi}(t - \Delta t) = \tilde{\varphi}_0 \exp \left[ \int_0^t dt' \bar{\gamma}(t') - \Delta t \bar{\gamma}(t) + \frac{\Delta t^2}{2} \bar{\gamma}'(t) + \dots \right]. \quad (22)$$

We will assume that this expansion can be truncated; the resulting solution will indeed turn out to satisfy  $\bar{\gamma}'(t) \ll 1$ , with all higher-order terms even smaller. Substituting (22) into (20), we obtain an implicit transcendental equation for  $\bar{\gamma}(t)$ :

$$\left(1 + \frac{\tau}{Z}\right) |\bar{\omega}_S| t = \frac{1}{2\sqrt{\pi}} \int_0^\infty d\Delta t \Delta t e^{-\Delta t \bar{\gamma}(t) - (\bar{\omega}_S^2 + 1)\Delta t^2 / 4} \left(\frac{q}{\epsilon} \bar{\omega}_S - 1\right). \quad (23)$$

This equation can be written in a compact form by invoking once again the plasma dispersion function (15): denoting  $\tilde{\gamma}(t) = \bar{\gamma}(t)/\sqrt{\bar{\omega}_S^2 + 1}$ , we get

$$\left(1 + \frac{\tau}{Z}\right) \sqrt{\pi} (\bar{\omega}_S^2 + 1) |\bar{\omega}_S| t = \left(\frac{q}{\epsilon} \bar{\omega}_S - 1\right) [1 + i\tilde{\gamma}(t) \mathcal{Z}(i\tilde{\gamma}(t))] \quad (24)$$

— effectively, a time-dependent dispersion relation, reminiscent of the PVG dispersion relation (16).

**3.2.1. Transient growth.** First of all, it is immediately clear from (23) that as time increases, (the real part of) the effective time-dependent growth rate  $\bar{\gamma}(t)$  must decrease and indeed go negative because the right-hand side has to keep up with the increasing left-hand side. Therefore, fluctuations will eventually decay. However, if  $\text{Re } \bar{\gamma}(t)$  is positive for some significant initial period of time, there can be a substantial transient amplification.

We can determine the time  $t_0$  when the transient growth ends by setting  $\text{Re } \tilde{\gamma}(t_0) = 0$  in (24). We immediately find that  $\text{Im } \tilde{\gamma}(t_0) = 0$  as well and that

$$t_0 = \frac{(q/\epsilon) \bar{\omega}_S - 1}{(1 + \tau/Z) \sqrt{\pi} (\bar{\omega}_S^2 + 1) |\bar{\omega}_S|}. \quad (25)$$

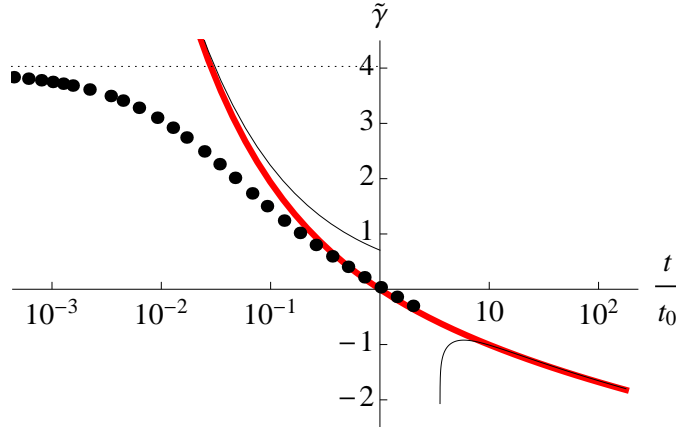


**Figure 4.** Time evolution of the effective growth rate: the red (bold) line is  $\tilde{\gamma}(t) = \gamma(t)/|k_{\parallel}|v_{\text{th}i}\sqrt{\bar{\omega}_S^2 + 1}$  obtained as a numerical solution of (26) and plotted vs.  $t/t_0$  (the time axis is logarithmic in base 10). The black (thin) lines are the asymptotics (27) and (32). The discrete points show the time evolution of the effective growth rate obtained in a direct linear numerical simulation using the gyrokinetic code *AstroGK* [36] with  $1/L_n = 1/L_T = 0$ ,  $q/\epsilon = 50$ ,  $\tau/Z = 1$ ,  $k_y\rho_i = 1$ ,  $k_{\parallel}v_{\text{th}i}/S = 0.5$ . The short-time-limit PVG growth rate for this case (obtained by solving (16)) is shown as a dotted horizontal line. The time is normalised using (25) for  $t_0$ . The time evolution of the perturbation amplitude for this case is shown in figure 1.

The dependence of  $t_0$  on  $k_y$  and  $k_{\parallel}$  — via  $\bar{\omega}_S = Sk_y\rho_i/k_{\parallel}v_{\text{th}i}$  and via the time normalisation factor of  $|k_{\parallel}v_{\text{th}i}|$  — tells us which modes grow longest. The interesting question, however, is rather which modes get maximally amplified during this transient growth.

*3.2.2. Maximal amplification.* The total amplification factor is given by  $e^N$ , where  $N = \int_0^{t_0} dt \tilde{\gamma}(t)$  is the number of exponentiations experienced by the mode during its growth period. In order to determine this, we need to know the time evolution of  $\tilde{\gamma}(t)$  up to  $t = t_0$ . Using (25), it is convenient to rewrite (24) as follows

$$\frac{t}{t_0} = 1 + i\tilde{\gamma} \mathcal{Z}(i\tilde{\gamma}). \quad (26)$$

When  $t \ll t_0$ , the solution is found by expanding the plasma dispersion function in  $\tilde{\gamma} \gg 1$ :

$$\frac{t}{t_0} \approx \frac{1}{2\tilde{\gamma}^2} \quad \Rightarrow \quad \tilde{\gamma} \approx \sqrt{\frac{t_0}{2t}}. \quad (27)$$

This asymptotic is not valid when  $t$  approaches  $t_0$ . More generally, (26) has a solution  $\tilde{\gamma} = \tilde{\gamma}(t/t_0)$ , whose functional form is independent of any parameters of the problem. It is plotted in figure 4 together with the asymptotic (27) and with a direct numerical solution showing how the transition between the short-time (§ 3.1) and long-time limits occurs. The amplification exponent is easily found:

$$N = \int_0^{t_0} dt \tilde{\gamma}(t) = t_0 \sqrt{\bar{\omega}_S^2 + 1} \int_0^1 d\xi \tilde{\gamma}(\xi) \approx 0.45 \frac{(q/\epsilon)\bar{\omega}_S - 1}{(1 + \tau/Z)\sqrt{\bar{\omega}_S^2 + 1}|\bar{\omega}_S|}, \quad (28)$$

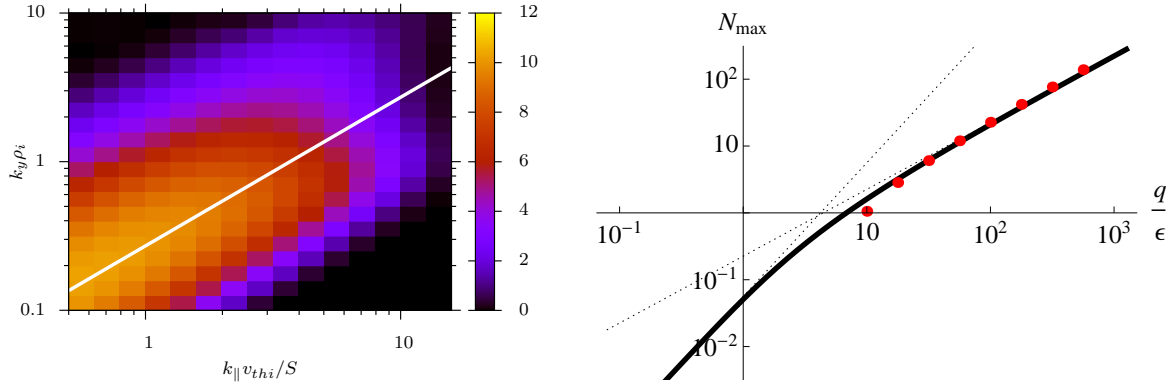


**Figure 5.** *Left panel:* The amplification exponent  $N$  vs.  $k_{\perp}$  and  $k_{\parallel}$  in the same *AstroGK* simulation as used to produce the discrete points in figure 4. The straight line shows the relationship between the wavenumbers given by the second formula in (29). *Right panel:* The maximum amplification exponent  $N_{\max}$  [ $N$  given by (28), maximised with respect to  $\bar{\omega}_S$ ] vs.  $q/\epsilon$ . The dotted lines show the  $q/\epsilon \gg 1$  asymptotic [see (29)] and the  $q/\epsilon \ll 1$  asymptotic, the latter straightforwardly obtained from (28):  $\bar{\omega}_S \approx 2(\epsilon/q)$ ,  $N_{\max} \approx 0.11(q/\epsilon)^2/(1 + \tau/Z)$  (but this is purely formal because the long-time conditions  $St_0 \gg 1$  and  $k_y\rho_i St_0 \gg 1$  will be broken in this regime, except for extremely long wavelengths). The discrete points show  $N_{\max}$  obtained via an *AstroGK* numerical parameter scan:  $k_{\parallel}v_{thi}/S = 0.5$ , varying  $k_{\perp}\rho_i$  and holding all other parameters fixed as in figure 4 (note that the asymptotic results do not in fact depend on  $k_{\parallel}$  or  $S$ , although the quality of the long-time asymptotic does).

where we have used (25) for  $t_0$  and computed the integral numerically. It is clear from (27) that the integral converges on its lower limit and is not dominated by it, so it does not matter that we cannot technically use (26) for short times.

According to (28),  $N$  depends on both wavenumbers via  $\bar{\omega}_S$  only (a plot of this dependence will be given in figure 8). Assuming  $q/\epsilon \gg 1$ , we find that the amplification exponent is maximised for  $\bar{\omega}_S \approx (\epsilon/q)^{1/3}$ , giving<sup>3</sup>

$$N_{\max} \approx 0.45 \frac{q/\epsilon}{1 + \tau/Z} \quad \text{for} \quad k_y\rho_i \approx \left(\frac{\epsilon}{q}\right)^{1/3} \frac{k_{\parallel}v_{thi}}{S}. \quad (29)$$

These results are illustrated in the left panel of figure 5. The amplification time for the maximally amplified modes identified in (29) is, from (25),

$$t_0 \approx \frac{q/\epsilon}{|k_{\parallel}|v_{thi}(1 + \tau/Z)\sqrt{\pi}} \approx \frac{(q/\epsilon)^{2/3}}{|Sk_y\rho_i|(1 + \tau/Z)\sqrt{\pi}}, \quad (30)$$

where we have restored dimensions to make explicit the dependence of  $t_0$  on  $k_{\parallel}$ .

Thus, we have learned that an entire family of modes, characterised by a particular (linear) relationship between  $k_y$  and  $k_{\parallel}$ , given in (29), will eventually enjoy the same net amplification, even though, as follows from the results of §3.1, they were not the fastest initially growing modes and some within this equally amplified family started off growing more slowly than others or even decaying. The more slowly growing modes are the

<sup>3</sup> Note that this is well outside of the wavenumber domain populated by the damped sound waves,  $\bar{\omega}_S < \epsilon/q$  (see Appendix B.1).

longer-wavelength ones and, according to (30), they compensate for their sluggishness with longer growth times.

Note that (30) confirms that the long-time limit is analytically reasonable because for large  $q/\epsilon$ , (30) formally satisfies  $k_y \rho_i St_0 \sim (q/\epsilon)^{2/3} \gg 1$  and also  $St_0 \gg 1$ , provided  $k_{\parallel} v_{\text{th}i}/S \ll q/\epsilon$ . The latter condition is marginally broken by the fastest initially growing modes: indeed, in §3.1, we saw that they had  $k_{\parallel} v_{\text{th}i}/S \sim 0.1q/\epsilon$ , so for them,  $St_0 \sim 3$ , not really a large number. For all longer-wavelength modes,  $t_0$  is safely within the domain of validity of the long-time limit.

Note also that, as we show at the end of Appendix B.1, the time-dependent dispersion relation (26) and its consequences derived above can be obtained directly from the PVG-instability dispersion relation (16) simply by restoring its  $k_x$  dependence, setting  $k_x = Sk_y t$ , taking the short-wavelength and long-time limit ( $k_x \rho_i \gg 1$ ,  $St \gg 1$ ), and assuming  $\epsilon/q \ll \bar{\omega}_S \ll 1$ . This calculation underscores the fundamental simplicity of the physics of the transient amplification: perturbations initially destabilised by the PVG are eventually swept by the perpendicular velocity shear into a stable region of the wavenumber space.

*3.2.3. Limits on short and long wavelengths.* We have seen that modes with parallel wavenumbers up to  $k_{\parallel} v_{\text{th}i}/S \sim q/\epsilon$  can be transiently amplified. From (29), we conclude that of these, the maximally amplified ones will have perpendicular wavenumbers up to  $k_y \rho_i \lesssim (q/\epsilon)^{2/3}$ , i.e.,  $k_y \rho_i$  can be relatively large — unlike in the short-time limit treated in §3.1, where the modes with  $k_y \rho_i \sim 1$  grew the fastest (although large  $k_y \rho_i$  were also unstable).

It should be understood that, while there is no ultraviolet cutoff in our theory that would limit the wavenumbers of the growing modes (in either direction), such a cutoff does of course exist in any real system. In the parallel direction, those  $k_{\parallel}$  that were strongly damped in the short-time limit (see (B.1)) are unlikely to recover in the long-time limit. In the perpendicular direction, the cutoff in  $k_y \rho_i$  will come from the collisional damping, which, in gyrokinetics, contains a spatial diffusion (see, e.g., [1]), and from the electron Landau damping, which we have lost by using the Boltzmann electron response (see (3)) and which should wipe out large  $k_y$  and  $k_{\parallel}$ .

On the infrared (long-wavelength) side of the spectrum, we have no cutoffs either. In a slab, these would be provided by the dimensions of the periodic box. In a real plasma, the cutoffs are set by the scales at which the system can no longer be considered homogeneous (in a tokamak, these are the equilibrium-gradient scale lengths and the minor radius for the perpendicular scales and the connection length  $qR$  for the parallel scales; we will need these considerations to fix transport scaling in §6).

*3.2.4. Significant amplification threshold.* If we maximise (28) without assuming  $q/\epsilon \gg 1$  (with the caveat that the long-time limit asymptotics are at best marginally valid then), we obtain a more general curve than (29), plotted in the right panel of

figure 5. We may define a critical threshold for significant amplification:  $N_{\max} = 1$  when  $q/\epsilon \approx 7$ . The role of this threshold will be discussed in §6.1.

*3.2.5. Long-time decay.* Finally, we obtain the long-time asymptotic decay law. Let us seek a solution of (26) such that  $t \gg t_0$  and  $\tilde{\gamma} \ll -1$ . Then

$$\frac{t}{t_0} \approx 2\sqrt{\pi} |\tilde{\gamma}| e^{\tilde{\gamma}^2} \Rightarrow \tilde{\gamma} \approx -\sqrt{\ln \frac{t}{t_0}}. \quad (31)$$

Since  $\tilde{\gamma}$  is only root-logarithmically large, the quality of this asymptotic is rather poor. If we insist on a more precise decay law, we can retain small corrections in (31) and get what turns out, upon a numerical test, to be a reasonably good approximation (see figure 4):

$$\tilde{\gamma} \approx -\sqrt{\ln \frac{t/(2\sqrt{\pi}t_0)}{\sqrt{\ln(t/2\sqrt{\pi}t_0)}}}. \quad (32)$$

For the maximally amplified modes (see (29)), the dimensional damping rate is  $\gamma(t) \approx |k_{\parallel}| v_{\text{thi}} \tilde{\gamma}(t)$  with  $t_0$  given by (30). This tells us that the decay is just slightly faster than exponential at the rate of order  $S$ . The longest-wavelength modes decay the slowest, after having being amplified the longest.

## 4. Solution including ITG

Let us now generalise the results obtained in §3 to include non-zero (i.e., non-negligible) density and temperature gradients. This means that we restore the terms involving  $\bar{\omega}_*$  and  $\eta_i$  in the general integral equation (11).

### 4.1. Short-time limit: the ITG-PVG dispersion relation

The short-time limit, introduced at the beginning of §3.1 for the case of pure PVG, is treated in an analogous fashion for the general ITG-PVG case. An analysis of the solutions of the resulting dispersion relation is useful in that its results assist physical intuition in ways relevant for some of the forthcoming discussion, but it is not strictly necessary for us to have them in order to work out how transient growth happens in the presence of the ITG drive. We have therefore relegated this analysis to Appendix B.2.

### 4.2. Long-time limit

We now continue in the same vein as in §3.2 and consider the long-time limit ( $St \gg 1$ ,  $k_y \rho_i St \gg 1$ ), in which we can simplify the kernels involving the Bessel functions in (11) by using (19) and also

$$\Lambda(\lambda, \lambda') \approx \frac{1}{2} - \frac{(\sqrt{\lambda} - \sqrt{\lambda'})^2}{2} \approx \frac{1}{2} - \frac{\bar{\omega}_S^2 \Delta t^2}{4}. \quad (33)$$

This allows us to rewrite (11) in the form that generalises (20):

$$\left(1 + \frac{\tau}{Z}\right) |\bar{\omega}_S| t \tilde{\varphi}(t) = \frac{1}{\sqrt{\pi}} \int_0^\infty d\Delta t e^{-(\bar{\omega}_S^2+1)\Delta t^2/4} \left\{ \left(\frac{q}{\epsilon} \bar{\omega}_S - 1\right) \frac{\Delta t}{2} - i\bar{\omega}_* \left[1 - \eta_i \left(\frac{1}{2} + \frac{(\bar{\omega}_S^2+1)\Delta t^2}{4}\right)\right] \right\} \tilde{\varphi}(t - \Delta t). \quad (34)$$

As in §3.2, we seek a solutions to this equation in the form (21), taking  $\Delta t \ll t$  and expanding the delayed potential under the integral according to (22). The result is the generalised form of (23):

$$\left(1 + \frac{\tau}{Z}\right) |\bar{\omega}_S| t = \frac{1}{\sqrt{\pi}} \int_0^\infty d\Delta t e^{-\Delta t \bar{\gamma}(t) - (\bar{\omega}_S^2+1)\Delta t^2/4} \left\{ \left(\frac{q}{\epsilon} \bar{\omega}_S - 1\right) \frac{\Delta t}{2} - i\bar{\omega}_* \left[1 - \eta_i \left(\frac{1}{2} + \frac{(\bar{\omega}_S^2+1)\Delta t^2}{4}\right)\right] \right\}. \quad (35)$$

Using again the plasma dispersion function (15) to express the time integrals and introducing the complex scaled frequency  $\tilde{\omega}(t) = i\bar{\gamma}(t)/\sqrt{\bar{\omega}_S^2+1}$ , we get

$$\begin{aligned} \left(1 + \frac{\tau}{Z}\right) \sqrt{\pi(\bar{\omega}_S^2+1)} |\bar{\omega}_S| t = & \left[ \frac{(q/\epsilon)\bar{\omega}_S - 1}{\sqrt{\bar{\omega}_S^2+1}} - \eta_i \bar{\omega}_* \tilde{\omega}(t) \right] [1 + \tilde{\omega}(t) \mathcal{Z}(\tilde{\omega}(t))] \\ & + (\eta_i - 1) \bar{\omega}_* \mathcal{Z}(\tilde{\omega}(t)), \end{aligned} \quad (36)$$

a time-dependent dispersion relation, which is the generalisation of (24).

*4.2.1. Transient growth.* The general argument that the real part of  $\bar{\gamma}(t)$  (i.e., the effective time-dependent growth rate) must eventually decrease and so fluctuations will, in the end, decay, applies to (35) similarly to the way it did to (23) (see §3.2.1), although this decay need not (and, as we will see, will not) be monotonic. The time  $t_0$  when the transient growth ends is now determined as follows. Let  $\text{Im} \tilde{\omega}(t_0) = 0$  and  $\tilde{\omega}(t_0) = \tilde{\omega}_0$  (real!). Then from (36) taken at  $t = t_0$ , we find the real frequency  $\tilde{\omega}_0$  by demanding that the imaginary part of the right-hand side vanish — this means that the coefficient in front of  $\mathcal{Z}(\tilde{\omega}_0)$  must be zero, because, for real  $\tilde{\omega}_0$ ,  $\text{Im} \mathcal{Z}(\tilde{\omega}_0) = \sqrt{\pi} e^{-\tilde{\omega}_0^2}$ . This condition gives

$$\eta_i \bar{\omega}_* \tilde{\omega}_0^2 - \frac{(q/\epsilon)\bar{\omega}_S - 1}{\sqrt{\bar{\omega}_S^2+1}} \tilde{\omega}_0 - (\eta_i - 1) \bar{\omega}_* = 0, \quad (37)$$

whence

$$\tilde{\omega}_0 = \frac{(q/\epsilon)\bar{\omega}_S - 1 \pm \sqrt{[(q/\epsilon)\bar{\omega}_S - 1]^2 + 4\eta_i(\eta_i - 1) \bar{\omega}_*^2 (\bar{\omega}_S^2 + 1)}}{2\eta_i \bar{\omega}_* \sqrt{\bar{\omega}_S^2 + 1}}. \quad (38)$$

Substituting this solution into the real part of (36) and taking advantage of the already enforced vanishing of the coefficient in front of  $\mathcal{Z}(\tilde{\omega}_0)$ , we get

$$t_0 = \frac{(q/\epsilon)\bar{\omega}_S - 1 + \sqrt{[(q/\epsilon)\bar{\omega}_S - 1]^2 + \eta_S^2 (1 - 1/\eta_i) \bar{\omega}_S^2 (\bar{\omega}_S^2 + 1)}}{2(1 + \tau/Z) \sqrt{\pi} (\bar{\omega}_S^2 + 1) |\bar{\omega}_S|}, \quad (39)$$

where we have replaced  $\eta_i^2 \bar{\omega}_*^2 = \eta_S^2 \bar{\omega}_S^2/4$  with  $\eta_S = v_{\text{th}i}/L_T S$  a new parameter that measures the strength of the ITG drive relative to the velocity shear. Note that we

picked the “−” mode in (38) because the “+” mode is not amplified ( $t_0 < 0$ , assuming  $\eta_i > 1$ ). Equation (39) is the generalisation of (25), to which it manifestly reduces when  $\eta_S = 0$  and with which it shares the property that the transient growth time depends on  $k_y$  and  $k_{\parallel}$  only via  $\bar{\omega}_S$  and the time normalisation factor  $|k_{\parallel}|v_{thi}$ .

*4.2.2. General dispersion relation.* We can now recast the general ITG-PVG case in a form that shows explicitly how it reduces to the case of pure PVG drive studied in § 3.2. First we note that the transient growth termination time (39) can be rewritten as

$$t_0 = \frac{1}{2} \left[ 1 + \sigma \sqrt{1 + \left(1 - \frac{1}{\eta_i}\right) \chi^2} \right] t_0^{(\text{PVG})}, \quad \chi = \frac{\eta_S \bar{\omega}_S \sqrt{\bar{\omega}_S^2 + 1}}{(q/\epsilon) \bar{\omega}_S - 1}, \quad (40)$$

where  $t_0^{(\text{PVG})}$  is given by (25),  $\eta_S \bar{\omega}_S = 2\eta_i \bar{\omega}_*$ ,  $\eta_S = v_{thi}/L_T S$  and  $\sigma = \text{sgn}[(q/\epsilon) \bar{\omega}_S - 1]$ .<sup>4</sup> Then the time-dependent dispersion relation (36) can be manipulated into the following form:

$$\left[ 1 + \sigma \sqrt{1 + \left(1 - \frac{1}{\eta_i}\right) \chi^2} \right] \frac{t}{t_0} = (2 - \chi \tilde{\omega}) [1 + \tilde{\omega} \mathcal{Z}(\tilde{\omega})] + \left(1 - \frac{1}{\eta_i}\right) \chi \mathcal{Z}(\tilde{\omega}). \quad (41)$$

The analogous equation for the case of pure PVG drive, (26), is recovered when  $\chi \ll 1$ , which means  $\eta_S \ll q/\epsilon$  (cf. (13)) and  $\eta_S \bar{\omega}_S \ll 1$ . In this limit, the behaviour of fluctuations in the presence of both PVG and ITG drives is well described by the results of § 3.2. Before discussing the general case, it is useful to consider the opposite extreme of weak velocity shear.

#### 4.3. Case of weak shear

Let  $\eta_S \gg q/\epsilon$  and  $\eta_S \bar{\omega}_S \gg 1$ , so  $\chi \gg 1$  (note that the same limit is also achieved for  $\bar{\omega}_S \rightarrow \infty$ ). Then the  $\chi$  dependence falls out of (41):

$$\frac{t}{t_0} = -\tilde{\omega} [1 + \tilde{\omega} \mathcal{Z}(\tilde{\omega})] + \mathcal{Z}(\tilde{\omega}), \quad (42)$$

where we have discarded the  $1/\eta_i$  terms by assuming  $\eta_i \gg 1$ . The transient growth termination time in this limit is, from (40),

$$t_0 = \frac{1}{2} \chi t_0^{(\text{PVG})} = \frac{\eta_S}{2(1 + \tau/Z) \sqrt{\pi(\bar{\omega}_S^2 + 1)}}. \quad (43)$$

When  $t \ll t_0$ , we find the solution of (42) by expanding in  $\tilde{\omega} \gg 1$ . It turns out that it consists of a large real frequency and an exponentially small growth rate: (42) becomes

$$\frac{t}{t_0} \approx -\frac{1}{2\tilde{\omega}} - i\sqrt{\pi} \tilde{\omega}^2 e^{-\tilde{\omega}^2} \quad \Rightarrow \quad \tilde{\omega} \approx -\frac{t_0}{2t} + i2\sqrt{\pi} \left(\frac{t_0}{2t}\right)^4 e^{-(t_0/2t)^2}. \quad (44)$$

More generally, for finite values of  $t/t_0$ , the solution of (42) is  $\tilde{\omega} = \tilde{\omega}(t/t_0)$ , with a functional form independent of the parameters of the problem. This solution is plotted in figure 6. It turns out that at  $t \approx 0.15 t_0$ , the growth rate increases sharply, reaches a

<sup>4</sup> If  $(q/\epsilon) \bar{\omega}_S < 1$ ,  $t_0^{(\text{PVG})} < 0$  and  $\chi < 0$ , but the ITG mode can still have transient growth,  $t_0 > 0$ .



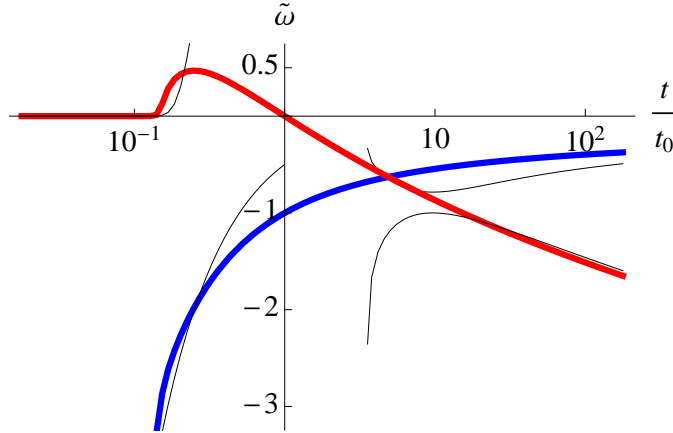


**Figure 6.** Time evolution of the effective growth rate and frequency: the red (upper bold) line is  $\tilde{\gamma}(t) = \text{Im} \omega(t)/|k_{\parallel}|v_{\text{th}i}\sqrt{\tilde{\omega}_S^2 + 1}$  and the blue (lower bold) line is  $\text{Re} \omega(t)/|k_{\parallel}|v_{\text{th}i}\sqrt{\tilde{\omega}_S^2 + 1}$ , both obtained as a numerical solution of (42) and plotted vs.  $t/t_0$  (the time axis is logarithmic<sub>10</sub>). The black (thin) lines show the growth rate and frequency given by the asymptotics (44) and (C.9) (the latter taken in the limit  $\chi \rightarrow \infty$  and  $\eta_i \rightarrow \infty$ ).

finite maximum and then decreases towards zero, which it reaches at  $t = t_0$ , whereupon growth turns to decay.<sup>5</sup>

Thus, there is a period of strong transient amplification, which lasts for a finite fraction of time  $t_0$ . The amplification exponent is

$$N = \int_0^{t_0} dt \tilde{\gamma}(t) = t_0 \sqrt{\tilde{\omega}_S^2 + 1} \int_0^1 d\xi \text{Im} \tilde{\omega}(\xi) \approx 0.057 \frac{\eta_S}{1 + \tau/Z}, \quad (45)$$

where we have used (43) and calculated the value of the integral under the curve in figure 6 numerically (note that since the growth rate is exponentially small at  $t \ll t_0$ , the precise lower integration limit is irrelevant). Remarkably, unlike in the case of the PVG drive (see (29)), the amplification exponent has no wavenumber dependence at all. Also unlike in the PVG case, it does depend on the shear and on the temperature gradient:  $N \propto \eta_S = v_{\text{th}i}/L_T S$ .

To recapitulate, we have found that, at low velocity shear, all modes are amplified by a large (and the same) factor before decaying eventually. Their transient amplification time is given by (43). Restoring dimensions, (43) and (45) are

$$t_0 \approx \frac{v_{\text{th}i}/(L_T S)}{2(1 + \tau/Z)\sqrt{\pi(S^2 k_y^2 \rho_i^2 + k_{\parallel}^2 v_{\text{th}i}^2)}}, \quad N \approx 0.057 \frac{v_{\text{th}i}/(L_T S)}{1 + \tau/Z}. \quad (46)$$

<sup>5</sup> This implies that perturbations first grow due to the ITG-PVG instability (at  $St \ll 1$ ), then slow down to exponentially small growth rates, then (at  $St \gg 1$ ) grow vigorously again before finally starting to decay at  $t = t_0$ . The intermediate period of virtually zero growth, which is a feature both of the weak-shear regime and of the general case (see § 4.4) and may appear strange at first glance, can be traced to the  $k_x$  dependence of ITG-PVG growth rates at long parallel wavelengths — this is explained in Appendix B.2.

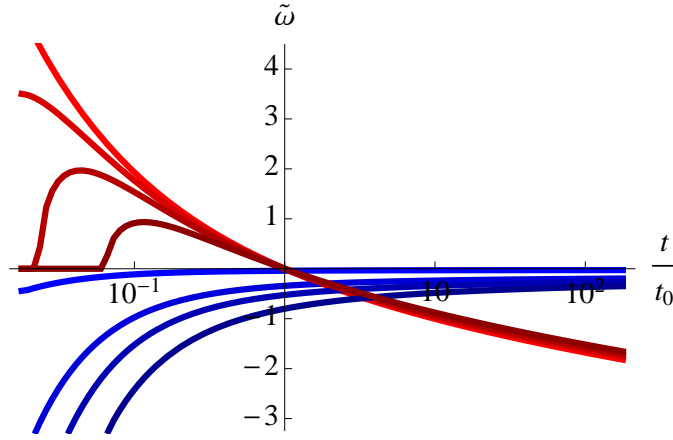


**Figure 7.** Effective normalised growth rates  $\text{Im} \tilde{\omega}(t/t_0)$  (red, top) and frequencies  $\text{Re} \tilde{\omega}(t/t_0)$  (blue, bottom) obtained via numerical solution of (41) with  $\eta_i = 5$  and  $\chi = 0.1, 1, 2, 10$  (from top/lighter to bottom/darker curves). See figure C1 for a more detailed depiction of the  $\chi = 1$  case (in Appendix C, where the functional form of these curves is derived analytically).

The transient growth lasts for a very long time at low  $S$  and the longest-growing modes are the long-wavelength ones. The limit  $S \rightarrow 0$  is singular in the sense that for arbitrarily small but non-zero  $S$  all modes eventually decay, while for  $S = 0$ , the indefinitely growing linear ITG instability is recovered ( $t_0 = \infty$ ,  $N = \infty$ ).

We have already made the point (in § 3.2.3) that while our theory does not limit the transiently growing wavenumbers from above, a fuller description of the plasma will.

#### 4.4. Case of finite shear

In the intermediate regimes between large and small  $\chi$  (i.e., weak and strong shear), the solutions of (41) transit from the weak-shear form described in § 4.3 to the pure-PVG case treated in § 3.2. Figure 7 shows the time-dependent growth rates and frequencies for several values of  $\chi$ . As  $\chi$  decreases (i.e.,  $S$  increases), the peak of the growth rate moves further into the past and the growth rate asymptotes to the pure-PVG case (figure 4). It is not hard to convince oneself analytically that this is indeed what ought to happen. Since intuitively it is rather obvious, further asymptotic considerations on this subject are exiled to Appendix C. The long-time decay asymptotic is also derived there (it is exactly analogous to that found in § 3.2.5).

Similarly to our previous calculations, the amplification exponent is

$$N(\bar{\omega}_S) = t_0(\bar{\omega}_S) \sqrt{\bar{\omega}_S^2 + 1} \int_0^1 d\xi \text{Im} \tilde{\omega}(\xi, \chi(\bar{\omega}_S)), \quad (47)$$

where  $\tilde{\omega}$  is the solution of (41). The wavenumber dependence enters via the  $\bar{\omega}_S$  dependence of  $t_0$  and of  $\chi$  (see (40)). The numerically computed amplification exponent as a function of  $\bar{\omega}_S$  and of  $\eta_S$  is plotted in the left panel of figure 8 for  $\eta_i = 5$  and  $q/\epsilon = 10$  (these are representative of the values encountered in the more realistic numerical studies of tokamak transport [7, 25, 26]). The pure-PVG case treated in § 3.2 remains a good

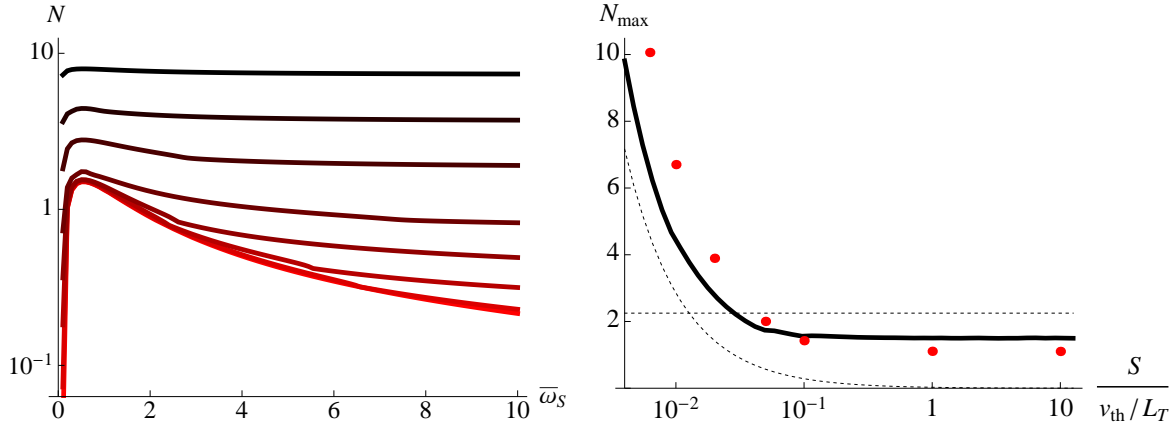


**Figure 8.** The amplification exponent  $N$ , given by (47) with  $\bar{\omega}$  the solution of (41) for  $\eta_i = 5$ ,  $q/\epsilon = 10$  and  $\tau/Z = 1$ . *Left panel:*  $N$  vs.  $\bar{\omega}_S$  for  $\eta_S = 1, 2, 5, 10, 20, 50, 100, 200$  (from bottom to top curves, in darkening shades of red). The numerical results for the same cases are shown in figure 9. The  $\eta_S = 0$  case (pure PVG drive) was virtually indistinguishable from  $\eta_S = 1$  when plotted (not shown here). The lowest- $\eta_S$  behaviour is well described by (28), the highest- $\eta_S$  by (45) (in the latter case, except for corrections associated with finite  $\eta_i$ , which are easy to compute if they are required). *Right panel:* The maximal amplification exponent  $N$  vs. the normalised shear ( $\eta_S^{-1} = SL_T/v_{thi}$ ). The maximum  $N(\bar{\omega}_S)$  is reached at  $\bar{\omega}_S \approx 0.54$ , independently of  $\eta_S$ . The dotted lines are the asymptotics (29) and (45). The finite offsets between the asymptotics and the exact curve are due to the fact that the asymptotics were calculated in the limits  $\eta_i \gg 1$  and  $q/\epsilon \gg 1$ , while for the exact solution we used relatively moderate values of these parameters. The discrete points show  $N_{\max}$  obtained via an *AstroGK* numerical parameter scan varying  $k_{\perp}\rho_i$  and  $S$  (i.e.,  $\eta_S$ ) while holding  $k_{\parallel}L_T = 0.02$  and the rest of the parameters fixed at the same values as quoted above.

approximation up to values of  $\eta_S$  of order 10. After that, there is a transition towards the weak-shear limit (§4.3), accompanied by the loss of wavenumber dependence as  $\eta_S$  is increased to values of order 100. The constant of proportionality between  $k_y$  and  $k_{\parallel}$  for the maximally amplified modes (i.e.,  $\bar{\omega}_S$  at which  $N$  is maximised) does not appear to depend on  $\eta_S$ , although at large  $\eta_S$ , the maximum is increasingly weak. The maximal amplification exponent is plotted in the right panel of figure 8. It is perhaps worth pointing out the qualitative similarity between this plot and figure 1 of Ref. [25], obtained from gyrokinetic simulations in full tokamak geometry.

Finally, the amplification exponent as a function of  $k_y$  and  $k_{\parallel}$ , obtained in direct (linear) numerical simulations, is shown in figure 9 (the parameters are the same as in the “theoretical” figure 8, left panel). The transition from the PVG curve (29) to the flat wavenumber dependence (45) is manifest, as are the limits of applicability of our approximations in the wavenumber space. Note the different normalisation of the parallel wavenumber here ( $k_{\parallel}L_T$ , characteristic of ITG) compared to the left panel of figure 5 ( $k_{\parallel}v_{thi}/S$ , characteristic of PVG). Hence the drift towards higher  $k_{\parallel}L_T$  as  $\eta_S = v_{thi}/SL_T$  decreases towards the PVG-dominated regime, where the parallel scale of maximally amplified modes is set by the shear rather than the temperature gradient.

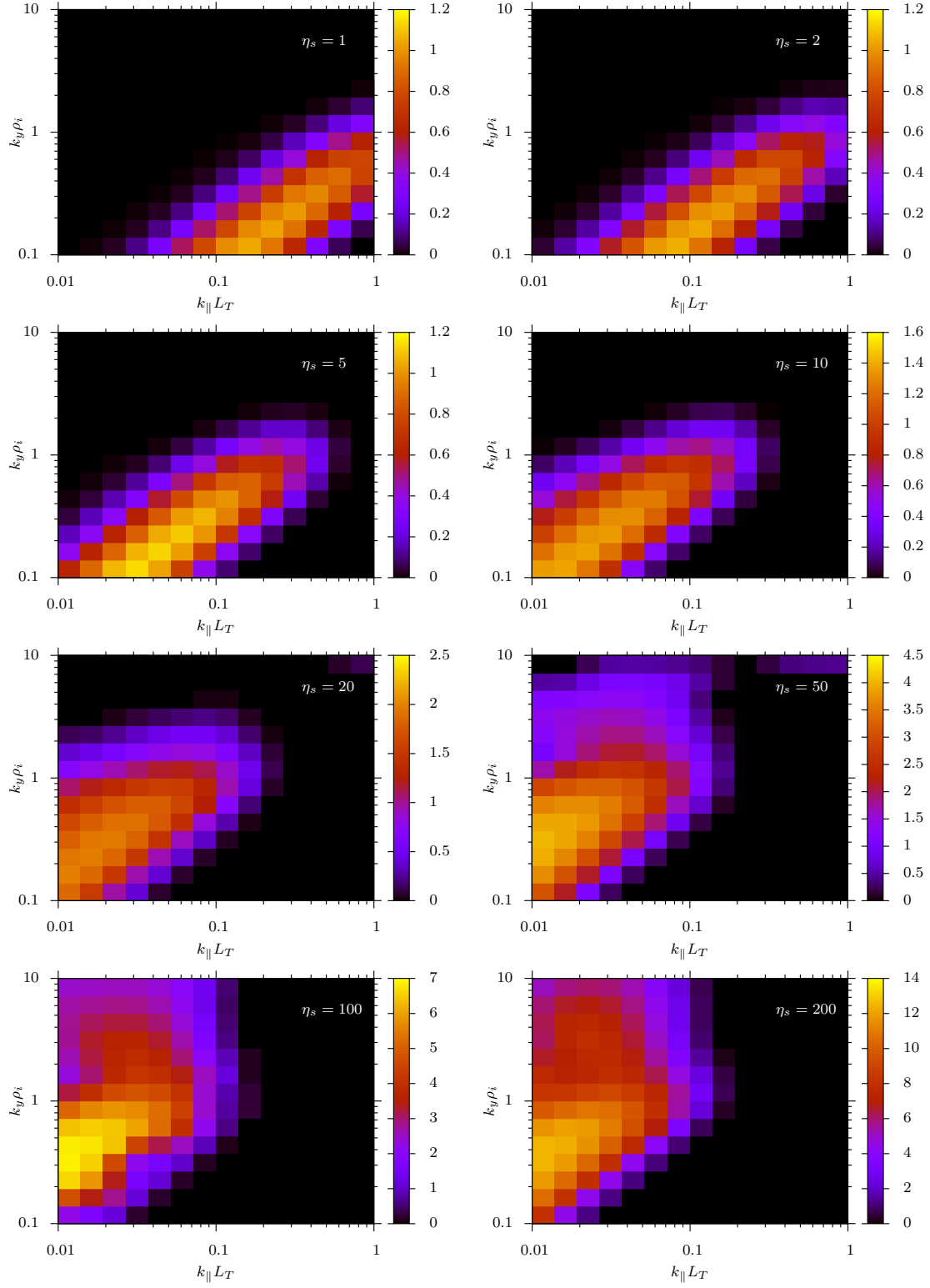


**Figure 9.** The amplification exponent  $N$  vs.  $k_{\parallel} L_T$  and  $k_y \rho_i$ , obtained numerically using *AstroGK* for the same parameters as the curves in the left panel of figure 8.

## 5. Qualitative summary of the linear results

In a gyrokinetic plasma with radial gradients of temperature and parallel velocity, both gradients are sources of free energy and so will drive the growth of fluctuations (ITG and PVG instabilities). The typical growth rate is of order  $\gamma \sim v_{thi}/L_T$  for ITG and  $\gamma \sim qS/\epsilon$  for PVG (see (18)), or the mean square of the two if they are comparable (see (B.10)). Because the mean plasma velocity is toroidal, it always has both a parallel and a perpendicular component (the latter a factor of  $q/\epsilon$  smaller than the former). The shear in the perpendicular ( $\mathbf{E} \times \mathbf{B}$ ) velocity is stabilising and causes all modes to decay eventually, so the fluctuation growth is transient — it is always transient in the limit, considered here, of zero magnetic shear and it is transient for large enough velocity shear  $S$  when the magnetic shear is finite [35, 7]. If the linear physics provides sufficiently vigorous and lasting amplification of finite initial perturbations, it is intuitively clear that the system must be able to sustain nonlinearly a saturated (subcritical) turbulent state (see §6). Therefore, the interesting question is how much transient amplification should be expected to occur and on what time scale.

In the preceding sections, we have addressed this question mathematically, with the results summarised by figures 5, 8 and 9 (see also (29), (30) and (46)). Very roughly, these results can be explained as follows. The effect of the perpendicular shear is to produce a secular increase with time of the radial wavenumber,  $k_x(t) \sim Sk_y t$ . When this becomes large enough, the instability is killed by Landau damping (see discussion at the end of Appendix B.1). If we estimate that this happens after  $t_0 \sim S^{-1}$  (i.e., for  $k_x(t_0)\rho_i \sim 1$ , assuming  $k_y\rho_i \sim 1$ ), we may conclude that initial perturbations will be amplified by a factor of  $e^N$ , where the amplification exponent is

$$N \sim \gamma t_0 \sim \frac{v_{thi}}{L_T S} \text{ for ITG} \quad \text{and} \quad N \sim \frac{q}{\epsilon} \text{ for PVG.} \quad (48)$$

Thus, the shear quenches the ITG amplification — but  $N$  cannot fall below the shear-independent level associated with the PVG (figure 8, right panel). This is indeed the case (see (29) and (46)), although, strictly speaking, one has to take into account the dependence of the quenching effect on the perpendicular and parallel wavenumbers — long-wavelength modes grow more slowly, but for a longer time; in the case of PVG, there is also a preferred relationship  $k_y\rho_i \sim (\epsilon/q)^{1/3}k_{\parallel}v_{thi}/S$  for the most strongly amplified modes (see §3.2 and figure 9). While these wavenumber dependences are likely to be important in the analysis of the resulting turbulent state and the associated transport, they effectively cancel out in the expression for the amplification exponent (because  $\gamma \propto k_y\rho_i$ ,  $t_0 \propto 1/k_y\rho_i$  at long wavelengths) and the results of the qualitative argument that we have given hold true.

It is instructive to compare these results with the conclusions of a long-wavelength fluid ITG-PVG theory presented in [35] (for the case of finite magnetic shear). In that regime, perpendicular shear, by effectively increasing  $k_x(t)$ , also caused eventual damping of the fluctuations, but this time via collisional viscosity. Therefore, to estimate the transient growth time  $t_0$ , one must set  $\gamma \sim \nu_{ii}k_x^2(t_0)\rho_i^2 \sim \nu_{ii}S^2k_y^2\rho_i^2t_0^2$ , where  $\nu_{ii}$  is

the ion collision rate. Then, ignoring wavenumber dependences again,  $t_0 \propto \gamma^{1/2} S^{-1}$ , so the amplification exponent is

$$N \sim \gamma t_0 \propto \frac{\gamma^{3/2}}{S} \propto \frac{1}{S} \text{ for ITG} \quad \text{and} \quad N \propto \sqrt{S} \text{ for PVG.} \quad (49)$$

Thus, the  $\mathbf{E} \times \mathbf{B}$  velocity shear again quenches the ITG instability, but once  $S$  is large enough for the PVG drive to take over, the amplification exponent actually grows as  $\sqrt{S}$ , the result obtained rigorously by [35] — in contrast with the shear-independent  $N \sim q/\epsilon$  that we have found in the kinetic regime. The practical conclusion from this is that it should be easier to obtain states of reduced transport [7, 25, 26, 37] in weakly collisional, kinetic plasmas.

## 6. Subcritical PVG turbulence and transport

While a detailed nonlinear theory is not the primary objective of this paper, we would like to give a preliminary, very crude and very heuristic discussion, inspired by the linear results presented above and by previous work on turbulence and transport scalings [8].

### 6.1. Turbulence threshold

Consider a situation when initial perturbations can grow transiently. The reason they decay eventually is that their radial wavenumber  $k_x(t)$  gets swept by the  $\mathbf{E} \times \mathbf{B}$  shear from the unstable to damped region (see discussion at the end of Appendix B.1 and at the end of Appendix B.2). If nonlinear interactions can scatter the energy from these modes back into the unstable region before they decay to small amplitudes beyond the reach of nonlinearity, then they can be transiently amplified once again and so on. Thus a nonlinear saturated state can be sustained — the subcritical PVG turbulence. This argument is entirely analogous to the standard paradigm for subcritical turbulence in hydrodynamic shear flows [44].

The typical time scale for the nonlinear interactions is the nonlinear decorrelation time  $\sim 1/k_\perp \delta v_E$ , where  $\delta v_E \sim k_\perp (c\varphi/B)$  is the fluctuating  $\mathbf{E} \times \mathbf{B}$  velocity. Therefore, in order to sustain turbulence the transient growth should last at least as long as one nonlinear decorrelation time:

$$t_0 \gtrsim \frac{1}{k_\perp \delta v_E}, \quad (50)$$

where  $t_0$  is the amplification time. In the saturated state, if it is sustained, the rate of amplification should be comparable to nonlinear decorrelation rate:

$$\gamma_{\text{eff}} \sim \frac{N}{t_0} \sim k_\perp \delta v_E, \quad (51)$$

where  $N$  is the amplification exponent. Combined with (50), this immediately implies, unsurprisingly, that the criterion for onset of turbulence is

$$N \gtrsim 1. \quad (52)$$

For subcritical turbulence, this criterion replaces the marginal stability condition  $\gamma = 0$ , usually employed for cases with well-defined eigenmodes. It is the “significant amplification threshold” introduced in §3.2.4. As we saw there, for PVG turbulence in a slab, it is equivalent to  $q/\epsilon \gtrsim 7$ . One might expect that much more sophisticated criteria could be derived by refining our arguments and testing these refinements against dedicated numerical parameter scans. The key conclusion is that  $q/\epsilon$  is now the critical parameter to be tuned and so magnetic configurations in which it is smaller may hold the promise of reduced or even completely suppressed ion turbulent transport (e.g., spherical tokamaks [39]).

## 6.2. Transport scalings

The standard mixing-length heuristics (often, somewhat misleadingly, referred to as “quasilinear” theory) are based on the argument that if fluctuations are driven by a linear instability with a characteristic growth rate  $\gamma$ , then they will saturate at amplitudes and scales such that the nonlinear decorrelation rate is comparable to this growth rate, viz.,  $k_\perp \delta v_E \sim \gamma$ . Then the turbulent heat diffusivity is  $\chi_T \sim \delta v_E / k_\perp \sim \gamma / k_\perp^2$  and so the ion heat flux is  $Q_i \sim \chi_T n_i T_i / L_T$ .

For subcritical fluctuations, there is no definite  $\gamma$ , but it is intuitive to argue, as we did in §6, that it should be replaced by  $\gamma_{\text{eff}} \sim N/t_0$ . For the PVG-driven fluctuations, we showed in §3.2.2 that, at maximal amplification,  $N \sim q/\epsilon$  and  $t_0 \sim (q/\epsilon)/k_\parallel v_{\text{th}i}$ , so (51) gives

$$\gamma_{\text{eff}} \sim k_\parallel v_{\text{th}i} \sim k_\perp \delta v_E. \quad (53)$$

This simple estimate is actually consistent with a very general idea that in systems with parallel propagation (or particle streaming) and perpendicular nonlinearity, turbulence tunes itself into a *critically balanced* state, viz., the time scales for these two effects are always comparable [24, 12, 41, 42, 34, 8]. We may now use the relationship (29) between  $k_\parallel$  and  $k_y$  for the maximally amplified modes to estimate  $k_\perp \rho_i \sim (\epsilon/q)^{1/3} k_\parallel v_{\text{th}i} / S$  and conclude, therefore, that

$$\chi_T \sim \frac{\gamma_{\text{eff}}}{k_\perp^2} \sim \rho_i^2 \frac{S^2}{k_\parallel v_{\text{th}i}} \left( \frac{q}{\epsilon} \right)^{2/3} \sim \frac{\rho_i^2 R S^2 q^{5/3}}{v_{\text{th}i} \epsilon^{2/3}}. \quad (54)$$

In the last expression, we have made another important assumption: since it is the longest-wavelength fluctuations that dominate transport, we should use the lowest parallel wavenumber possible in a tokamak:  $k_\parallel \sim 1/qR$ , where  $R$  is the major radius. This prescription was proposed in [8] for ITG turbulence. In a sense, it is even more natural here than it was there because, in the theory developed in the preceding sections, the wavelengths of maximally amplified modes are not limited from above by any microscale physics — if we took the slab model literally, the limit would be the periodicity length of the box; in a tokamak, the connection length is a natural choice.

Finally, under this scheme, the ion heat flux scales as<sup>6</sup>

$$\frac{Q_i}{n_i T_i v_{thi}} \sim \frac{\chi_T}{v_{thi} L_T} \sim \left( \frac{S}{\Omega_i} \right)^2 \frac{q^{5/3}}{\epsilon^{2/3}} \frac{R}{L_T}. \quad (55)$$

One fairly obvious feature of the scalings (54) and (55) (independent of most of the specific assumptions that we made in deriving them) is that the heat diffusivity is independent of the temperature gradient and so heat transport is not very “stiff” — the relevant comparison is with the scaling for the ITG regime,  $Q_i \propto q(R/L_T)^3$  [8]. A softening of transport in the presence of velocity shear has indeed been reported both in experimental [32, 33] and in numerical [7, 25, 26] studies. Physically, it is not surprising: as the driver of the turbulence in this regime is the PVG, not the ITG, steeper temperature gradients do not produce stronger turbulence and so the positive feedback loop between  $R/L_T$  and the heat diffusivity is broken.

## Acknowledgments

We gratefully acknowledge many inspiring discussions with M Barnes, J Connor, N Loureiro, F Parra, C Roach and especially W Dorland. Some of these interactions were made possible by the Leverhulme Trust International Network for Magnetised Plasma Turbulence. Some of the work reported herein was done at the Isaac Newton Institute, Cambridge, during the programme “Gyrokinetics in Laboratory and Astrophysical Plasmas” (2010). Numerical simulations were carried out at HPC-FF (Jülich) and HECTOR (Edinburgh). AAS was supported in part by the STFC Grant ST/F002505/2. EGH was supported by an EPSRC CASE studentship in partnership with the Euratom/CCFE Association. The views and opinions expressed herein are unlikely to reflect those of the European Commissioners. EGH was also supported in part by the Thematic Programme “Gyrokinetics for ITER” at the Wolfgang Pauli Institute, Vienna (2011).

<sup>6</sup> There is a number of reasons to take these specific scaling predictions with a grain of salt. Besides making the assumptions stated above, we have ignored many effects that may be important and may change our estimates of the relevant scales, times and amplitudes: the role of zonal flows in regulating and/or sustaining the turbulence, the possibility that the effective radial and poloidal wavenumbers,  $k_x$  and  $k_y$ , are not the same in a system with imposed velocity shear, the role of magnetic shear if it is present, various geometry (curvature) effects etc. It is also not necessary, although intuitive and possibly supported by numerical evidence [26], that the relationship (29) between  $k_{\parallel}$  and  $k_y$  obtained by maximising the linear amplification should persist in the nonlinear regime, especially if the system is far above the significant amplification threshold (§ 6.1). There are several possible alternative theories that can be constructed in a similar vein to that presented above, but the current state of numerical and experimental evidence does not yet allow us to differentiate between them in a falsifiable fashion. Future investigations will focus on this task. Preliminary numerical studies suggest that far from the significant amplification threshold (§ 6.1), the ion heat flux does not in fact scale as strongly with  $q$  as suggested by (55) (E G Highcock 2011, unpublished).



## Appendix A. Low-Mach-number local gyrokinetics in a rotating axisymmetric plasma

Here we describe the version of the gyrokinetic system of equations appropriate for a rotating axisymmetric plasma, which is the starting point for our calculation. For a detailed derivation, we refer the reader to [2] (earlier treatments are [4, 43, 38]).

We consider the axisymmetric rotating equilibrium and work in the subsidiary low-Mach-number limit, as described at the beginning of §2. The distribution function of particles of species  $s$  is written in the following form

$$f_s(\mathbf{r}, \mathbf{v}) = \left[ 1 - \frac{Z_s e \varphi(\mathbf{r})}{T_s} \right] F_{0s}(\psi(\mathbf{R}_s), \varepsilon_s) + F_{1s}(\mathbf{R}_s, \varepsilon_s, \mu_s, \sigma_{\parallel}) + h_s(\mathbf{R}_s, \varepsilon_s, \mu_s, \sigma_{\parallel}), \quad (\text{A.1})$$

Let us explain the numerous notation that appears here. The standard 6D kinetic position-and-velocity phase space  $(\mathbf{r}, \mathbf{v})$  is transformed to the 5D gyrokinetic phase space, where the dynamics are averaged over the Larmor orbits and so do not depend on the gyroangle. If  $\mathbf{w} = \mathbf{v} - \mathbf{u}$  is peculiar velocity with respect to the mean flow,  $B$  is the magnitude of the mean magnetic field,  $\hat{\mathbf{b}} = \mathbf{B}/B$  its direction,  $\Omega_s = Z_s e B / m_s c$  the cyclotron frequency,  $Z_s e$  is particle charge ( $Z_e = -1$ ),  $m_s$  particle mass,  $c$  the speed of light, then the gyrokinetic variables  $(\mathbf{R}_s, \varepsilon_s, \mu_s, \sigma_{\parallel})$  are defined as follows: the guiding centre position  $\mathbf{R}_s = \mathbf{r} - \hat{\mathbf{b}} \times \mathbf{w} / \Omega_s$ , the energy variable  $\varepsilon_s = m_s w^2 / 2$  (this is only correct in the low- $M$  limit), the magnetic moment  $\mu_s = m_s w_{\perp}^2 / 2B$ , and the sign of the parallel velocity  $\sigma_{\parallel} = w_{\parallel} / |w_{\parallel}|$  (the subscripts  $\perp$  and  $\parallel$  refer to the mean-field direction  $\hat{\mathbf{b}}$ ). In (A.1), the particle distribution function is split into the mean Maxwellian, which can be shown to depend only on the flux label  $\psi(\mathbf{R}_s)$  via the mean density  $n_s$  and mean temperature  $T_s$ , namely,<sup>7</sup>

$$F_{0s}(\psi(\mathbf{R}_s), \varepsilon_s) = n_s(\psi(\mathbf{R}_s)) \left[ \frac{m_s}{2\pi T_s(\psi(\mathbf{R}_s))} \right]^{3/2} \exp \left[ -\frac{\varepsilon_s}{T_s(\psi(\mathbf{R}_s))} \right], \quad (\text{A.2})$$

the mean perturbed distribution function  $F_{1s}$ , which contains collisional (classical and neoclassical) effects and will not concern us here, the Boltzmann response containing the perturbed scalar potential  $\varphi$ , and the guiding-centre distribution function  $h_s$ .

If we take the mean fields  $\mathbf{B}$  (i.e.,  $\psi$  and  $I(\psi)$ ),  $n_s(\psi)$ ,  $T_s(\psi)$  and  $\omega(\psi)$  to be known and the fluctuations about them to be purely electrostatic, then the latter are fully described by a closed system containing the gyrokinetic evolution equation for  $h_s$  and the quasineutrality condition determining  $\varphi$ :

$$\begin{aligned} \frac{\partial h_s}{\partial t} + [\mathbf{u}(\mathbf{R}_s) + w_{\parallel} \hat{\mathbf{b}} + \mathbf{V}_d + \langle \mathbf{V}_E \rangle_{\mathbf{R}_s}] \cdot \frac{\partial h_s}{\partial \mathbf{R}_s} &= \frac{Z_s e F_{0s}}{T_s} \left[ \frac{\partial}{\partial t} + \mathbf{u}(\mathbf{R}_s) \cdot \frac{\partial}{\partial \mathbf{R}_s} \right] \langle \varphi \rangle_{\mathbf{R}_s} \\ &- (\langle \mathbf{V}_E \rangle_{\mathbf{R}_s} \cdot \nabla \psi) \left[ \frac{d \ln n_s}{d \psi} + \left( \frac{\varepsilon_s}{T_s} - \frac{3}{2} \right) \frac{d \ln T_s}{d \psi} + \frac{B_{\phi} m_s w_{\parallel} R}{B T_s} \frac{d \omega}{d \psi} \right] F_{0s}, \end{aligned} \quad (\text{A.3})$$

<sup>7</sup> Establishing the Maxwellian equilibrium depends on the plasma being sufficiently collisional, namely, that the collision frequency is not smaller than the fluctuation frequency by more than one order in the gyrokinetic expansion parameter. The density being a function solely of  $\psi$  only holds in the low- $M$  limit.

$$\left( \sum_s \frac{Z_s^2 e^2 n_s}{T_s} \right) \varphi = \sum_s Z_s e \int d^3 \mathbf{w} \langle h_s \rangle_{\mathbf{r}}, \quad (\text{A.4})$$

where  $w_{\parallel} = \sigma_{\parallel} \sqrt{2(\varepsilon_s - \mu_s B)}$ ,  $B_{\phi} = I(\psi)/R$  is the azimuthal magnetic field,  $\mathbf{V}_d = (c/Z_s e B) \hat{\mathbf{b}} \times (m_s w_{\parallel}^2 \hat{\mathbf{b}} \cdot \nabla \hat{\mathbf{b}} + \mu_s \nabla B)$  is the magnetic drift velocity,  $\mathbf{V}_E = (c/B) \hat{\mathbf{b}} \times \nabla \varphi$  is the  $\mathbf{E} \times \mathbf{B}$  velocity, and the gyroaverages are defined

$$\langle \varphi \rangle_{\mathbf{R}_s} = \frac{1}{2\pi} \int_0^{2\pi} d\vartheta \varphi(\mathbf{R}_s + \hat{\mathbf{b}} \times \mathbf{w}/\Omega_s) \quad (\text{function of } \mathbf{R}_s), \quad (\text{A.5})$$

$$\langle h_s \rangle_{\mathbf{r}} = \frac{1}{2\pi} \int_0^{2\pi} d\vartheta h_s(\mathbf{r} - \hat{\mathbf{b}} \times \mathbf{w}/\Omega_s, \varepsilon_s, \mu_s, \sigma_{\parallel}) \quad (\text{function of } \mathbf{r} \text{ and } \mathbf{w}). \quad (\text{A.6})$$

Note that we suppressed the collision term in (A.3) (formally, we are ordering the collision frequency small via a subsidiary expansion).

The approximation of Boltzmann electrons amounts to setting  $h_e = 0$  in (A.4).

#### Appendix A.1. Local Cartesian frame in the case of zero magnetic shear

Let us take the mean magnetic field to be locally straight and uniform, so it has constant magnitude, no curvature and no shear. This means that the magnetic drifts vanish ( $\mathbf{V}_d = 0$ ) and we can introduce a local orthogonal Cartesian coordinate system (see figure 2):

$$\hat{\mathbf{x}} = \frac{\nabla \psi}{B_p R}, \quad \hat{\mathbf{y}} = \frac{\hat{\mathbf{b}} \times \nabla \psi}{B_p R}, \quad \hat{\mathbf{z}} = \hat{\mathbf{b}}, \quad (\text{A.7})$$

where  $B_p = |\nabla \psi|/R$  is the poloidal component of  $\mathbf{B}$ . We will view this coordinate system as having its origin ( $x = 0$ ) at some reference flux surface  $\psi_0$ , so in the vicinity of this flux surface,  $\psi \approx \psi_0 + x B_p R$ . Then

$$\mathbf{u} = \omega(\psi) R^2 \nabla \psi = \omega(\psi) R \left( \frac{B_{\phi}}{B} \hat{\mathbf{z}} + \frac{B_p}{B} \hat{\mathbf{y}} \right) \approx \left[ \omega R + x B_p R^2 \frac{d\omega}{d\psi} \right] \left( \frac{B_{\phi}}{B} \hat{\mathbf{z}} + \frac{B_p}{B} \hat{\mathbf{y}} \right), \quad (\text{A.8})$$

where all quantities in the last expression are taken at  $\psi = \psi_0$  and  $B_{\phi} = I(\psi)/R$  is the azimuthal component of  $\mathbf{B}$ . We have only retained the spatial dependence of  $\omega$  (in the form of a Taylor expansion) because we are formally ordering velocity gradients as  $O(1/M)$ , while all other mean fields are assumed to have  $O(1)$  variation on the system scale. The constant part of the velocity can be removed by going to a frame moving (azimuthally) at this velocity. The  $z$  component of the velocity shear can be neglected because it multiplies  $\partial/\partial z$  in (A.3) and we order  $x$  as small (in the gyrokinetic expansion parameter) compared to the parallel scale of the fluctuations, whereas the  $y$  component of the shear remains important because it multiplies  $\partial/\partial y \gg \partial/\partial z$ . It follows that the velocity field can be replaced by the linear shear flow as stated in (1).

Given the shearing box approximation described above and the assumption of Boltzmann electrons ( $h_e = 0$ ), the conversion of (A.3) and (A.4) into (2) and (3) is straightforward. Note that  $(c/B)(T_i/Z_e) = v_{\text{thi}}^2/2\Omega_i = \rho_i v_{\text{thi}}/2$ , where  $\rho_i = v_{\text{thi}}/\Omega_i$  is the ion Larmor radius.

## Appendix B. PVG and ITG-PVG dispersion relations

Here we provide some elementary analytical considerations of the linear dispersion relations that govern the early evolution of the fluctuations.

### Appendix B.1. PVG dispersion relation

In the pure PVG case, the dispersion relation is (16), containing the well-known PVG instability [11] and the sound wave. The following considerations provide some analytical support for figure 3.

*Marginal stability threshold.* This is easy to obtain analytically without any approximation: at the threshold,  $\text{Im} \bar{\omega} = 0$  and then, from (16), the real frequency is readily shown to vanish as well, so we get  $(q/\epsilon)\bar{\omega}_S = (1 + \tau/Z)/\Gamma_0(\lambda)$ . Thus, we have an instability if<sup>8</sup>

$$\frac{k_{\parallel} v_{\text{th}i}}{qS/\epsilon} < \frac{k_y \rho_i \Gamma_0(\lambda)}{1 + \tau/Z} \lesssim \frac{0.66}{1 + \tau/Z}, \quad (\text{B.1})$$

where  $\lambda = k_y^2 \rho_i^2 / 2$  (see figure 3, right panel). The second inequality in (B.1) implies that there is an absolute finite limit on the parallel wavenumbers at which the PVG instability can survive (reached for  $k_y \rho_i \approx 1.26$ ).

*PVG modes and sound waves.* The growing modes have no real frequency. In fact, there is no real frequency as long as  $(q/\epsilon)\bar{\omega}_S > 1$ , which means that the mode is purely decaying between  $(q/\epsilon)\bar{\omega}_S = 1$  and the marginal stability boundary  $(q/\epsilon)\bar{\omega}_S = (1 + \tau/Z)/\Gamma_0(\lambda) > 1$  (see (B.1)). For  $(q/\epsilon)\bar{\omega}_S < 1$ , the mode turns into a damped sound wave (this is shown in the left panel of figure 3). Thus, the PVG drive has pushed the sound waves into a wedge in wavenumber space,

$$k_y \rho_i < \frac{k_{\parallel} v_{\text{th}i}}{qS/\epsilon} \quad (\text{B.2})$$

(see figure 3, right panel) and populated the rest with nonpropagating growing or decaying modes.

*Growth at long parallel wavelengths.* Looking for unstable solutions in the long-wavelength limit ( $k_{\parallel} v_{\text{th}i}/S \ll 1$ ), we consider the asymptotic form of (16) with  $\bar{\omega} = i\bar{\gamma}$  (pure growth) and  $\bar{\gamma} \gg 1$ , when  $1 + i\bar{\gamma} \mathcal{Z}(i\bar{\gamma}) \approx 1/2\bar{\gamma}^2$ . Then the growing solution is

$$\bar{\gamma} \approx \sqrt{\frac{(q/\epsilon)\bar{\omega}_S - 1}{2[(1 + \tau/Z)/\Gamma_0(\lambda) - 1]}} \Rightarrow \gamma \approx \sqrt{\frac{(qS/\epsilon)k_y \rho_i k_{\parallel} v_{\text{th}i}}{2[(1 + \tau/Z)/\Gamma_0(\lambda) - 1]}}. \quad (\text{B.3})$$

<sup>8</sup> If  $qS/\epsilon > 0$ , the unstable mode has either  $k_y > 0$ ,  $k_{\parallel} > 0$  or  $k_y < 0$ ,  $k_{\parallel} < 0$  (see figure B1 and discussion in Appendix B.2); if  $qS/\epsilon < 0$ , then  $k_y$  and  $k_{\parallel}$  have to have opposite signs. We can assume without loss of generality that all these quantities are positive.

In the second expression, we have restored dimensions and assumed  $(q/\epsilon)\bar{\omega}_S \gg 1$  (which ensures  $\bar{\gamma} \gg 1$  and is consistent with the short-time ordering adopted at the beginning of §3.1). Note that, while this asymptotic has a peak at  $k_y \rho_i \sim 1$ , it does not capture the maximum growth rate because of its monotonic increase with  $k_{\parallel}$ . The maximum growth rate is, in fact, reached for  $\bar{\gamma} \sim 1$ , where the plasma dispersion function does not yield itself to a simple asymptotic expansion. The numerical solution is shown in figure 3.

*Growth at short perpendicular wavelengths.* Finally, we note that one can obtain a good approximate preview of the results of §3.2 if one restores the dependence on  $k_x$  by setting  $\lambda = (k_x^2 + k_y^2)/2$  in (16). The effect of the perpendicular shear is to increase the instantaneous  $k_x$  of the mode, so the limit of short perpendicular wavelengths (or, more precisely, large  $k_x$  but finite  $k_y$ ) is similar to the limit of long times. Since  $\Gamma_0(\lambda) \approx 1/\sqrt{2\pi\lambda}$  for  $\lambda \gg 1$ , (16) becomes (assuming also  $k_y \rho_i \gg k_{\parallel} v_{thi}/(qS/\epsilon)$ , i.e., we are far outside the domain of the damped sound waves discussed above):

$$\left(1 + \frac{\tau}{Z}\right) \sqrt{\pi} \frac{k_{\parallel} v_{thi}}{qS/\epsilon} \sqrt{1 + \frac{k_x^2}{k_y^2}} \approx \frac{1}{St_0} \sqrt{1 + \frac{k_x^2}{k_y^2}} \approx 1 + i\bar{\gamma}\mathcal{Z}(i\bar{\gamma}), \quad (\text{B.4})$$

where  $t_0$  is given by (25), but with dimensions restored (i.e., not normalised by  $k_{\parallel} v_{thi}$ ) and  $\epsilon/q \ll \bar{\omega}_S \ll 1$  (as will be the case for the most strongly amplified modes in §3.2.2). This formula has two interesting consequences.

Firstly, setting  $k_x = Sk_y t$  and  $St \ll 1$ , we recover the time-dependent dispersion relation (26) and so the transient growth and eventual decay of the fluctuations derived more formally in §3.2 (without the assumption  $\epsilon/q \ll \bar{\omega}_S \ll 1$ ). Thus, there is a smooth connection between the short-time and long-time behaviour of the PVG-driven fluctuations. Note that applying the same asymptotics to (B.3), we recover (27). That the PVG growth rate must be extinguished at large enough  $k_x$  is also obvious from the instability criterion (B.1), where increasing  $\lambda$  eventually breaks the first inequality.

Secondly, in the short-time but also short-perpendicular-wavelength limit ( $k_x \ll k_y$  but  $k_y \rho_i \gg 1$ ), the growth rate of the PVG instability is independent of  $k_y$ , as is indeed manifest in figure 3.

## Appendix B.2. ITG-PVG dispersion relation

In the short-time limit, we can, analogously to the derivation in §3.1, reduce the integral equation (11) to a dispersion relation for the normalised complex frequency  $\bar{\omega} = \omega/|k_{\parallel}|v_{thi}$ :

$$\frac{1 + \tau/Z}{\Gamma_0(\lambda)} - 1 = \left(\frac{q}{\epsilon} \bar{\omega}_S - 1 - \eta_i \bar{\omega}_* \bar{\omega}\right) [1 + \bar{\omega} \mathcal{Z}(\bar{\omega})] + \eta_i \bar{\omega}_* \left[\frac{3}{2} - \Lambda(\lambda) - \frac{1}{\eta_i}\right] \mathcal{Z}(\bar{\omega}), \quad (\text{B.5})$$

where  $\Gamma_0(\lambda) = e^{-\lambda} I_0(\lambda)$  and  $\Lambda(\lambda) = 1 - \lambda + \lambda I_1(\lambda)/I_0(\lambda)$ ; we recapitulate the definitions of  $\lambda = k_y^2 \rho_i^2/2$ ,  $\bar{\omega}_S = Sk_y \rho_i/k_{\parallel} v_{thi}$ ,  $\bar{\omega}_* = k_y \rho_i/2|k_{\parallel}|L_n$  and  $\eta_i = L_n/L_T$ . This is the standard slab ITG-PVG dispersion relation for an unsheared gyrokinetic plasma.

*Marginal stability thresholds.* The way in which ITG and PVG coexist is easiest to understand by examining the marginal stability thresholds. Setting  $\text{Im } \bar{\omega} = 0$ ,  $\bar{\omega} = \text{Re } \bar{\omega} = \bar{\omega}_0$  and demanding that the imaginary part of (B.5) vanish, we get the equation for the real frequency of the mode at marginal stability:

$$\eta_i \bar{\omega}_* \bar{\omega}_0^2 - \left( \frac{q}{\epsilon} \bar{\omega}_S - 1 \right) \bar{\omega}_0 - \eta_i \bar{\omega}_* \left[ \frac{3}{2} - \Lambda(\lambda) - \frac{1}{\eta_i} \right] = 0. \quad (\text{B.6})$$

Substituting the solution of this equation back into (B.5), we arrive at the marginal stability condition:

$$\eta_i^2 \bar{\omega}_*^2 \left[ \frac{3}{2} - \Lambda(\lambda) - \frac{1}{\eta_i} \right] + \left[ \frac{1 + \tau/Z}{\Gamma_0(\lambda)} - 1 \right] \left[ \frac{q}{\epsilon} \bar{\omega}_S - \frac{1 + \tau/Z}{\Gamma_0(\lambda)} \right] = 0. \quad (\text{B.7})$$

Since  $\eta_i \bar{\omega}_* = k_y \rho_i / 2 |k_{\parallel}| L_T$  and  $\bar{\omega}_S = S k_y \rho_i / k_{\parallel} v_{\text{thi}}$ , the above equation can be solved for the two curves in the  $(k_{\parallel}, k_y)$  plane that enclose the unstable region:

$$k_{\parallel} L_{uT} = \frac{k_y \rho_i \eta_u^2}{2 \sqrt{1 + \eta_u^2}} \frac{[3/2 - \Lambda(\lambda) - 1/\eta_i] / [(1 + \tau/Z)/\Gamma_0(\lambda) - 1]}{\left\{ -1 \pm \sqrt{1 + \eta_u^2 [3/2 - \Lambda(\lambda) - 1/\eta_i] / [1 - \Gamma_0(\lambda)/(1 + \tau/Z)]} \right\}}, \quad (\text{B.8})$$

where  $L_{uT} = v_{\text{thi}} / \sqrt{(qS/\epsilon)^2 + (v_{\text{thi}}/L_T)^2} = (qS/\epsilon) \sqrt{1 + \eta_u^2}$  is a convenient normalisation of the parallel wavenumber for the mixed ITG-PVG regime and  $\eta_u = (v_{\text{thi}}/L_T)/(qS/\epsilon) = \eta_S/(q/\epsilon)$  is a parameter that measures the relative strength of the ITG and PVG drives.

The pure PVG regime is  $\eta_u \ll 1$ , in which case the “+” curve above turns into (B.1) (which is perhaps easier to infer directly from (B.7)), while the “−” curve is simply  $k_{\parallel} = 0$  — these demarcate two symmetric PVG-unstable regions at  $k_{\parallel} > 0, k_y > 0$  and  $k_{\parallel} < 0, k_y < 0$  (assuming  $S > 0$ ). The pure ITG regime is  $\eta_u \gg 1$ , in which case  $L_{uT} = L_T$  and

$$k_{\parallel} L_T = \pm k_y \rho_i \sqrt{\frac{3/2 - \Lambda(\lambda) - 1/\eta_i}{4 [(1 + \tau/Z)/\Gamma_0(\lambda) - 1/2]^2 - 1}}. \quad (\text{B.9})$$

These curves enclose four symmetric ITG-unstable regions in the four quadrants of the  $(k_{\parallel}, k_y)$  plane. In the general case of finite  $\eta_u$ , when both ITG and PVG drives play a role, these drives combine constructively in the PVG-unstable quadrants  $k_{\parallel} > 0, k_y > 0$  and  $k_{\parallel} < 0, k_y < 0$ , whereas in the remaining two quadrants, the stable PVG mode, which is just a PVG-modified sound wave (cf. (17)), has a stabilising influence on the ITG drive.

*Solutions.* It is not hard to show that the solutions of the ITG-PVG dispersion relation (B.5) can be expressed in the general form, which is a direct generalisation of (18):

$$\omega = \sqrt{(qS/\epsilon)^2 + (v_{\text{thi}}/L_T)^2} f(k_y \rho_i, k_{\parallel} L_{uT}; \eta_u, \eta_i). \quad (\text{B.10})$$

The growth rate  $\gamma = \text{Im } \omega$ , obtained numerically for a typical situation with finite  $\eta_u$ , is shown in figure B1, as are the marginal stability thresholds (B.8), (B.9) and (B.1). Note that in general the ITG-PVG mode also has a real frequency. Note also that the solutions of the general ITG-PVG dispersion relation retain the PVG-mode property

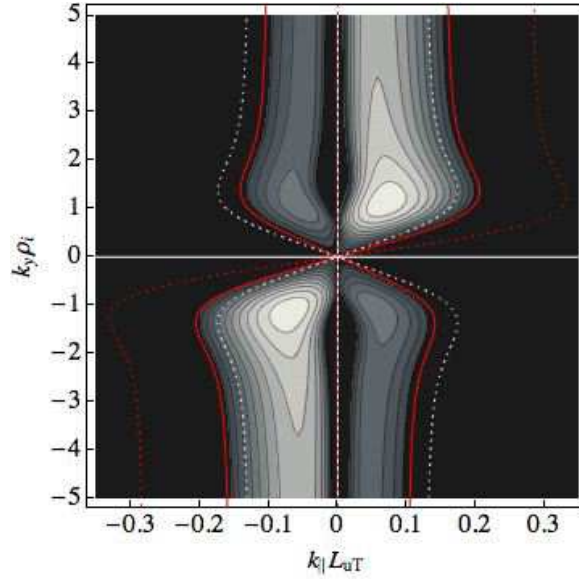


**Figure B1.** The ITG-PVG growth rate  $\gamma/\sqrt{(qS/\epsilon)^2 + (v_{thi}/L_T)^2}$  vs.  $k_{\parallel}L_{uT}$  and  $k_y\rho_i$ , where  $L_{uT} = v_{thi}/\sqrt{(qS/\epsilon)^2 + (v_{thi}/L_T)^2}$ . In this plot,  $\eta_u = (v_{thi}/L_T)/(qS/\epsilon) = 5$ ,  $\eta_i = 5$  and  $\tau/Z = 1$ . Only positive values are plotted, black means  $\gamma < 0$ . The red curves show the stability boundary (B.8), the red dotted curves the pure-PVG ( $\eta_u \rightarrow 0$ ) stability boundary (B.1) and the white dotted curve the pure-ITG ( $\eta_u \rightarrow \infty$ ) stability boundary (B.9). See figure B2 for cuts along the  $k_y\rho_i$  axis for some representative values of  $k_{\parallel}L_{uT}$ .

of independence of  $k_y$  at short perpendicular wavelengths. This is easily demonstrated analytically by taking the limit  $k_y\rho_i \gg 1$ ,  $k_{\parallel}L_{uT}$  in (B.5) — all factors of  $k_y\rho_i$  then cancel on both sides of the equation.

*Growth at long parallel wavelengths.* To assist physical intuition and some of the forthcoming discussion, it is useful to consider the ITG-PVG dispersion relation in the “fluid” limit,  $\bar{\omega} \gg 1$  (case of long parallel wavelengths). Expanding  $\mathcal{Z}(\bar{\omega}) = -1/\bar{\omega} - 1/2\bar{\omega}^3 - 3/4\bar{\omega}^5 + \dots$ , we recast (B.5) as a cubic equation

$$2 \left[ \frac{1 + \tau/Z}{\Gamma_0(\lambda)} - 1 \right] \bar{\omega}^3 + 2\eta_i\bar{\omega}_* \left[ 1 - \Lambda(\lambda) - \frac{1}{\eta_i} \right] \bar{\omega}^2 + \left( \frac{q}{\epsilon} \bar{\omega}_S - 1 \right) \bar{\omega} - \eta_i\bar{\omega}_* \left[ \Lambda(\lambda) + \frac{1}{\eta_i} \right] = 0. \quad (\text{B.11})$$

If we also consider long perpendicular wavelengths,  $\lambda \rightarrow 0$ , and assume  $\eta_i \gg 1$ , we get

$$\frac{2\tau}{Z} \bar{\omega}^3 + \left( \frac{q}{\epsilon} \bar{\omega}_S - 1 \right) \bar{\omega} - \eta_i\bar{\omega}_* = 0. \quad (\text{B.12})$$

The long-wavelength PVG instability (17) is recovered as a balance of the first two terms (in the limit  $\eta_u \ll 1$ ); the fluid version of the ITG instability obtains from the balance of the first and third terms (when  $\eta_u \gg 1$ ):

$$\bar{\omega}^3 \approx \frac{Z}{2\tau} \eta_i\bar{\omega}_* \quad \Rightarrow \quad \omega \approx (k_{\parallel}^2 c_s^2 \eta_i \omega_*)^{1/3} \quad (\text{B.13})$$

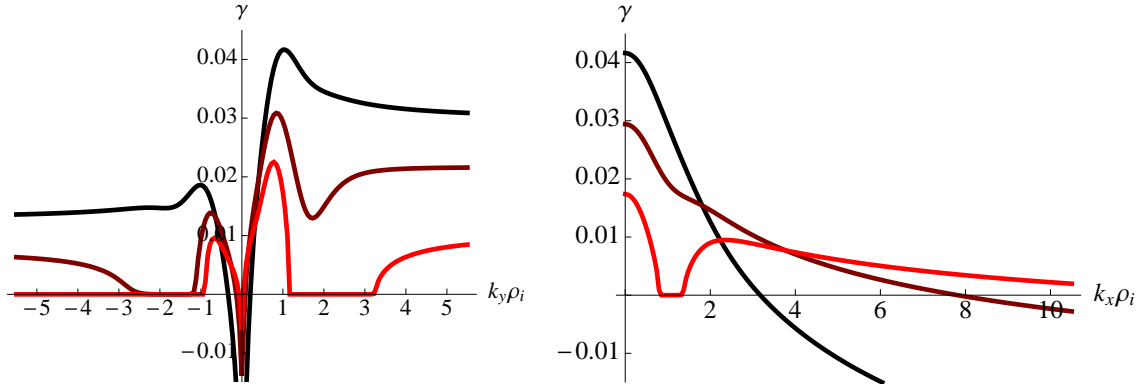


**Figure B2.** *Left panel:* The ITG-PVG growth rate, calculated numerically from (B.5) for the same parameters and normalised in the same way as in figure B1, vs.  $k_y \rho_i$ . The three curves are for  $k_{\parallel} L_{uT} = 0.01$  (red), 0.02 (brown) and 0.05 (black). *Right panel:* Same, but vs.  $k_x \rho_i$ .

(three roots, one real, two complex, of which one unstable).

Analysing the long-wavelength dispersion relation in great detail is not a useful exercise because it turns out to be a very poor quantitative approximation to (B.5) in most parameter regimes. It does, however, make transparent how the ITG and PVG modes coexist. It also helps understand qualitatively what is perhaps a somewhat obscure property of the ITG (and ITG-PVG) mode: if the parallel wavenumber is held fixed and low ( $k_{\parallel} L_{uT} \ll 1$ ), the mode is unstable at long perpendicular wavelengths ( $\lambda \ll 1$ ), becomes stabilised at finite  $\lambda$ , and then reignites at larger  $\lambda$ . This is because the “fluid” ITG solution (B.13) depends on the cancellation  $\Lambda(\lambda \rightarrow 0) \approx 1$  (and the limit  $\eta_i \gg 1$ ) in the second term of (B.11). As  $\lambda$  increases, this second term becomes larger than the first and the mode is stabilised (or, more precisely, it still has an exponentially small growth rate originating from the  $i\sqrt{\pi} e^{-\bar{\omega}^2}$  term in  $\mathcal{Z}(\bar{\omega})$ , neglected in the derivation of (B.11) — this comes from the Landau pole and is not recoverable in fluid theories). The instability is rekindled at larger  $\lambda$  because the coefficient in the first (cubic) term in (B.11) grows ( $\sim \sqrt{\lambda}$  as  $\lambda \rightarrow \infty$ ) and comes back into play (although the approximation  $\bar{\omega} \gg 1$  breaks down simultaneously).

This behaviour, calculated from the full dispersion relation (B.5), is illustrated in figure B1. In the right panel of this figure, we show the growth rate dependence on  $k_x \rho_i$ , the dependence on which we have restored by setting  $\lambda = (k_x^2 + k_y^2) \rho_i^2 / 2$  (similarly to what was done at the end of Appendix B.1). The attenuation and subsequent resumption of growth as the perpendicular wavenumber grows is the origin of similar behaviour, but as a function of time, seen in the long-time limit of the ITG-PVG transient growth in § 4 and Appendix C — because the effect of the perpendicular shear is to increase gradually the instantaneous  $k_x$  of the mode. At long parallel wavelengths, as time increases, the mode first grows (when  $St \ll 1$ ), then slows down for a while, then (at  $St \gg 1$ ) the growth is resumed for another period and finally extinguished at  $t = t_0$ .

### Appendix C. Transient growth with finite shear

Here we provide some asymptotic considerations that back up the behaviour of the time-dependent growth rates and frequencies described in §4.4.

As in §4.3, when  $t \ll t_0$ , we may expand the time-dependent dispersion relation (41) assuming large frequency  $\tilde{\omega} \gg 1$ , which is mostly real ( $\tilde{\gamma} \equiv \text{Im } \tilde{\omega} \ll \text{Re } \tilde{\omega}$ ):

$$\left[ 1 + \sigma \sqrt{1 + \left(1 - \frac{1}{\eta_i}\right) \chi^2} \right] \frac{t}{t_0} \approx - \left(1 - \frac{2}{\eta_i}\right) \frac{\chi}{2\tilde{\omega}} - \frac{1}{\tilde{\omega}^2} + i\sqrt{\pi} (2 - \chi\tilde{\omega}) \tilde{\omega} e^{-\tilde{\omega}^2}. \quad (\text{C.1})$$

The two terms on the right-hand side that involve  $\chi$  are the ITG terms and the other two are the PVG terms. When the latter or the former predominate, we recover the limiting cases treated in §4.3 and §3.2, respectively (in the case of strong PVG-driven growth the resonant term should be dropped as the growth rate is not small). The transition between the two regimes can be understood essentially by calculating finite- $\chi$  corrections.

*Strong ITG, weak PVG.* Let us first consider the case where  $\chi\tilde{\omega} \gg 1$  but  $\chi \sim 1$ . Then the two PVG terms on the right-hand side of (C.1) can be dropped and we obtain the following solution

$$\tilde{\omega} \approx - \frac{(1 - 2/\eta_i)\chi}{1 + \sigma\sqrt{1 + (1 - 1/\eta_i)\chi^2}} \frac{t_0}{2t}, \quad \tilde{\gamma} \approx \frac{2\sqrt{\pi}}{1 - 2/\eta_i} \tilde{\omega}^4 e^{-\tilde{\omega}^2}, \quad (\text{C.2})$$

a straightforward generalisation of (44), to which it reduces when  $\chi \rightarrow \infty$  and  $\eta_i \rightarrow \infty$  (there is, of course, no problem retaining finite  $\eta_i$ , it was assumed large in §4.3 merely to make the algebra more compact). The exponentially small growth rate  $\tilde{\gamma}$  stops being exponentially small and takes off to order-unity values when the frequency  $\tilde{\omega}$  stops being large and becomes  $\tilde{\omega} \sim 1$ . It is evident from (C.2) that this happens at earlier times for smaller  $\chi$ . Hence the behaviour of the growth rates and frequencies shown in figure 7: the peak growth moves into the past (smaller  $t/t_0$ ) as  $\chi$  decreases. The effect of finite  $\chi$  is only noticeable when  $\chi^2 \sim 1$ ; at larger values, the frequency is basically independent of  $\chi$  and so the weak-shear limit ( $\chi \rightarrow \infty$ ; §4.3) applies.

*Strong PVG, weak ITG.* Let us now restore the PVG terms in (C.1). This becomes necessary when  $\chi\tilde{\omega} \sim 1$  or smaller. In this limit and in neglect of the exponentially small resonant term, the solution of (C.1) is

$$\tilde{\omega} \approx - \frac{\chi}{8} \left(1 - \frac{2}{\eta_i}\right) \frac{t_0^{(\text{PVG})}}{t} \pm i \sqrt{\frac{t_0^{(\text{PVG})}}{2t} - \left[ \frac{\chi}{8} \left(1 - \frac{2}{\eta_i}\right) \frac{t_0^{(\text{PVG})}}{t} \right]^2}, \quad (\text{C.3})$$

where, to make the formula more compact, we have used the first expression in (40) to express the left-hand side of (C.1) in terms of  $t_0^{(\text{PVG})}$ . Here we are assuming  $(q/\epsilon)\bar{\omega}_S > 1$ , so  $\sigma = 1$ ,  $t_0^{(\text{PVG})} > 0$  and  $\chi > 0$ .



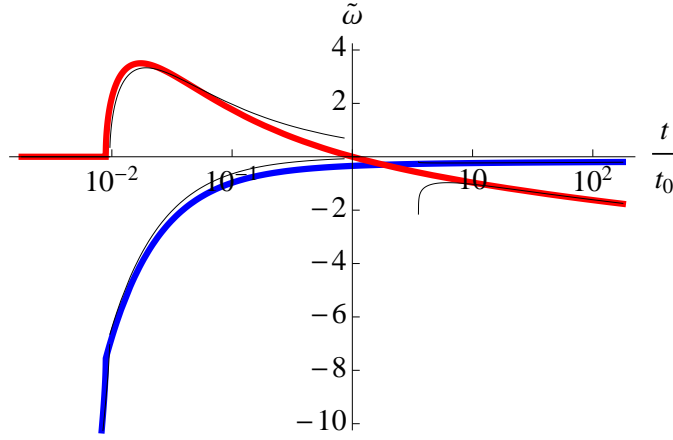


**Figure C1.** Effective normalised growth rate  $\text{Im}\tilde{\omega}(t/t_0)$  (red, top) and frequency  $\text{Re}\tilde{\omega}(t/t_0)$  (blue, bottom) obtained via numerical solution of (41) with  $\eta_i = 5$  and  $\chi = 1$ . This is one of the cases already shown in figure 7, replotted here to compare with the analytic solutions derived in Appendix C: the black (thin) lines show the (combined) growth asymptotics (C.3) and (C.6) for  $t/t_0 \ll 0$  (the growth rate (C.7) is so small that it is zero for all practical purposes) and the decay asymptotic (C.9) for  $t/t_0 \gg 1$ .

The “+” branch in (C.3) is a growing mode and is a direct generalisation of (27). The difference with the pure-PVG case is that growth does not extend indefinitely into the past, but requires

$$\frac{t}{t_0^{(\text{PVG})}} > \frac{\chi^2}{32} \left(1 - \frac{2}{\eta_i}\right)^2. \quad (\text{C.4})$$

At longer times, the growth rates increases, reaches its maximum value

$$\tilde{\gamma}_{\text{max}} = \frac{2}{\chi(1 - 2/\eta_i)} \quad \text{at} \quad \frac{t}{t_0^{(\text{PVG})}} = \frac{\chi^2}{16} \left(1 - \frac{2}{\eta_i}\right)^2, \quad (\text{C.5})$$

and then asymptotes to the pure-PVG case (27). At shorter times, the frequency (C.3) becomes purely real (asymptoting eventually to  $\tilde{\omega}$  given by (C.2)). To get the growth rate in this regime, we must restore the resonant term in (C.1), which gives an exponentially small growth rate. The (growing) solution now is

$$\tilde{\omega} \approx -\frac{\chi}{8} \left(1 - \frac{2}{\eta_i}\right) \frac{t_0^{(\text{PVG})}}{t} - \sqrt{\left[\frac{\chi}{8} \left(1 - \frac{2}{\eta_i}\right) \frac{t_0^{(\text{PVG})}}{t}\right]^2 - \frac{t_0^{(\text{PVG})}}{2t}}, \quad (\text{C.6})$$

$$\tilde{\gamma} \approx \frac{\sqrt{\pi}(2 + \chi|\tilde{\omega}|)|\tilde{\omega}|^3 e^{-\tilde{\omega}^2}}{\sqrt{\left[\chi(1 - 2/\eta_i)t_0^{(\text{PVG})}/8t\right]^2 - t_0/2t}}. \quad (\text{C.7})$$

Figure C1 shows the numerical solution of (41) together with the asymptotics (C.3), (C.6) and (C.7), all calculated for  $\chi = 1$  and  $\eta_i = 5$ . Even though the asymptotics are only technically valid for  $\chi \lesssim 1/\tilde{\omega} \ll 1$ , we see that they in fact work rather well even for moderate finite  $\chi$  (this is due to the accumulation of numerically small prefactors

that multiply  $\chi$  in the above expressions). For values of  $\chi$  significantly larger than unity, this agreement breaks down and one has to use (C.2).

Thus, we have learned that both PVG- and ITG-dominated transient growth is exponentially weak at very short times, then increases to large or finite values before slackening again and turning to decay at  $t = t_0$ . At what time the transition happens and how large  $\tilde{\gamma}$  can get depends on  $\chi$ . Recalling the definition of  $\chi$  (see (40)), we note that larger values of  $\chi$  are achieved for stronger shear (i.e.,  $\eta_S$  larger compared to  $q/\epsilon$ ), larger  $k_y \rho_i$  or smaller  $k_{\parallel} v_{\text{th}i}/S$  (i.e., larger  $\bar{\omega}_S$ ). Thus, the transition between the ITG and PVG regimes happens non-uniformly in the wavenumber space (as, indeed, is evident in the middle panel of figure 8).

We remind the reader that all of the above is only valid in the long-time limit,  $\bar{\omega}_S t \gg 1, k_y \rho_i$  (see the beginning of § 3.2), which means that for some wavenumbers and/or values of  $\eta_S$  and  $q/\epsilon$ , the transition from exponentially small to finite growth rate may be superseded by the transition from the short- to long-time limit, i.e., the initial ITG-PVG instability may not have time to peter out (due to increase in  $k_{\perp} \rho_i$  caused by shearing; see Appendix B.2) before being rekindled again by the transient growth.

*Long-time decay.* Finally, to complete our treatment of the general ITG-PVG case, let us consider the eventual decay of the fluctuations. This is done in exactly the same way as in § 3.2.5. In the limit  $t \gg t_0$ , we assume again that  $\tilde{\omega} = i\tilde{\gamma}$ , where  $\tilde{\gamma}$  is large, negative and mostly real. Then (41) is approximated by

$$\left[ 1 + \sigma \sqrt{1 + \left(1 - \frac{1}{\eta_i}\right) \chi^2} \right] \frac{t}{t_0} \approx 2\sqrt{\pi} (2 + i\chi|\tilde{\gamma}|) |\tilde{\gamma}| e^{\tilde{\gamma}^2} \quad \Rightarrow \quad \tilde{\gamma} \approx -\sqrt{\ln \frac{t}{t_0}}, \quad (\text{C.8})$$

so, like in (31), we have a root-log law, i.e., the decay of the modes with time is just barely super-exponential. As before, (C.8) is a quantitatively poor approximation except at ridiculously long times and a better one can be obtained by retaining corrections. This way we also obtain the (decaying with time) real frequency. The result is

$$\tilde{\gamma} \approx -\sqrt{\ln \left[ \frac{1 + \sqrt{1 + (1 - 1/\eta_i)\chi^2}}{\sqrt{4 + \chi^2 \ln(t/(2\sqrt{\pi} t_0))}} \frac{t/(2\sqrt{\pi} t_0)}{\sqrt{\ln(t/(2\sqrt{\pi} t_0))}} \right]}, \quad \tilde{\omega} \approx -\frac{\arctan(\chi|\tilde{\gamma}|/2)}{2|\tilde{\gamma}|}. \quad (\text{C.9})$$

For  $\chi \ll 1$ , we recover the pure-PVG result (32). For  $\chi \gg 1$  and  $\eta_i \gg 1$  (the weak-shear limit), these asymptotics are shown in figure 6 and for  $\chi = 1$  and  $\eta_i = 5$  in figure C1.

## References

- [1] Abel I G, Barnes M, Cowley S C, Dorland W and Schekochihin A A 2008 *Phys. Plasmas* **15** 122509
- [2] Abel I G, Plunk G G, Wang E, Barnes M, Cowley S C, Dorland W and Schekochihin A A 2011 *Plasma Phys. Control. Fusion* submitted
- [3] Artun M and Tang W M 1992 *Phys. Fluids B* **4** 1102
- [4] Artun M and Tang W M 1994 *Phys. Plasmas* **1** 2682

- [5] Artun M, Reynders J V W and Tang W M 1993 *Phys. Fluids B* **5** 4072
- [6] Barnes M, Abel I G, Dorland W, Ernst D R, Hammett G W, Ricci P, Rogers B N, Schekochihin A A and Tatsuno T 2009 *Phys. Plasmas* **16** 072107
- [7] Barnes M, Parra F I, Highcock E G, Schekochihin A A, Cowley S C and Roach C M 2011 *Phys. Rev. Lett.* **106** 175004
- [8] Barnes M, Parra F I and Schekochihin A A 2011 *Phys. Rev. Lett.* **107** 115003
- [9] Casson F J, Peeters A G, Camenen Y, Hornsby W A, Snodin A P, Strintzi D and Szepesi G 2009 *Phys. Plasmas* **16** 092303
- [10] Catto P J, Bernstein I B and Tessarotto M 1987 *Phys. Fluids* **30** 2784
- [11] Catto P J, Rosenbluth M N and Liu C S 1973 *Phys. Fluids* **16** 1719
- [12] Cho J and Lazarian A 2004 *Astrophys. J.* **615** L41
- [13] Connor J W, Cowley S C, Hastie R J and Pan L R 1987 *Plasma Phys. Control. Fusion* **29** 919
- [14] Connor J W and Martin T J 2007 *Plasma Phys. Control. Fusion* **49** 1497
- [15] Coppi B, Rosenbluth M N and Sagdeev R Z 1967 *Phys. Fluids* **10** 582
- [16] Cowley S C and Bishop C M 1986 *Culham Laboratory Report CLM-M* 109
- [17] Cowley S C, Kulsrud R M and Sudan R 1991 *Phys. Fluids B* **3** 2767
- [18] Dimits A M, Bateman G, Beer M A, Cohen B I, Dorland W, Hammett G W, Kim C, Kinsey J E, Kotschenreuther M, Kritz A H, Lao L L, Mandrekas J, Nevins W M, Parker S E, Redd A J, Shumaker D E, Sydora R and Weiland J 2000 *Phys. Plasmas* **7** 969
- [19] Dimits A M, Cohen B I, Nevins W M and Shumaker D E 2001 *Nucl. Fusion* **41** 1725
- [20] Dong J Q and Horton W 1993 *Phys. Fluids B* **5** 1581
- [21] Dorland W, Kotschenreuther M, Beer M A, Hammett G W, Waltz R E, Dominguez R R, Valanju P M, Miner Jr. W H, Dong J Q, Horton W, Waelbroeck F L, Tajima T and LeBrun M J 1994 *Plasma Phys. Controlled Nucl. Fusion Res.* **3** 463
- [22] Fried B D and Conte S D 1961 *The Plasma Dispersion Function* (New York: Academic Press)
- [23] Goldreich P and Lynden-Bell D 1965 *Mon. Not. R. Astron. Soc.* **130** 125
- [24] Goldreich P and Sridhar S 1995 *Astrophys. J.* **438** 763
- [25] Highcock E G, Barnes M, Schekochihin A A, Parra F I, Roach C M and Cowley S C 2010 *Phys. Rev. Lett.* **105** 215003
- [26] Highcock E G, Barnes M, Parra F I, Schekochihin A A, Roach C M and Cowley S C 2011 *Phys. Plasmas* **18** 102304
- [27] Hinton F L and Wong S K 1985 *Phys. Fluids* **28** 3082
- [28] Kinsey J E, Waltz R E and Candy J 2005, *Phys. Plasmas* **12** 062302
- [29] Kinsey J E, Waltz R E and Candy J 2006, *Phys. Plasmas* **13** 022305
- [30] Kotschenreuther M, Dorland W, Beer M A and Hammett G W 1995, *Phys. Plasmas* **2** 2381
- [31] Linsker R 1981 *Phys. Fluids* **24** 1485
- [32] Mantica P, Strintzi D, Tala T, Giroud C, Johnson T, Leggate H, Lerche E, Loarer T, Peeters A G, Salmi A, Sharapov S, Van Eester D, de Vries P C, Zabeo L and Zastrow K-D 2009 *Phys. Rev. Lett.* **102** 175002
- [33] Mantica P, Angioni C, Challis C, Colyer G, Frassinetti L, Hawkes N, Johnson T, Tsalias M, de Vries P C, Weiland J, Baiocchi B, Beurskens M N A, Figueiredo A C A, Giroud C, Hobirk J, Joffrin E, Lerche E, Naulin V, Peeters A G, Salmi A, Sozzi C, Strintzi D, Staebler G, Tala T, Van Eester D and Versloot T 2011 *Phys. Rev. Lett.* **107** 135004
- [34] Nazarenko S V and Schekochihin A A, *J. Fluid Mech.* **677** 134
- [35] Newton S L, Cowley S C and Loureiro N F 2010 *Plasma Phys. Control. Fusion* **52** 125001
- [36] Numata R, Howes G G, Tatsuno T, Barnes M and Dorland W 2010 *J. Comput. Phys.* **229** 9347
- [37] Parra F I, Barnes M, Highcock E G, Schekochihin A A and Cowley S C 2011 *Phys. Rev. Lett.* **106** 115004
- [38] Peeters A G, Strintzi D, Camenen Y, Angioni C, Casson F J, Hornsby W A and Snodin A P 2009 *Phys. Plasmas* **16** 042310
- [39] Roach C M, Abel I G, Akers R J, Arter W, Barnes M, Camenen Y, Casson F J, Colyer G, Connor

- J W, Cowley S C, Dickinson D, Dorland W, Field A R, Guttenfelder W, Hammett G W, Hastie R J, Highcock E, Loureiro N F, Peeters A G, Reshko M, Saarelma S, Schekochihin A A, Valovic M and Wilson H R 2009 *Plasma Phys. Control. Fusion* **51** 124020
- [40] Rudakov L I and Sagdeev R Z 1961 Dokl. Acad. Nauk SSSR **138** 581
- [41] Schekochihin A A, Cowley S C, Dorland W, Hammett G W, Howes G G, Plunk G G, Quataert E and Tatsuno T 2008, *Plasma Phys. Control. Fusion* **50** 124024
- [42] Schekochihin A A, Cowley S C, Dorland W, Hammett G W, Howes G G, Quataert E and Tatsuno T 2009, *Astrophys. J. Suppl.* **182** 310
- [43] Sugama H and Horton W 1997 *Phys. Plasmas* **4** 405
- [44] Trefethen L N, Trefethen A E, Reddy S C and Driscoll T A 1993, *Science* **261** 578
- [45] Waelbroeck F L, Antonsen T M Jr, Guzdar P N and Hassam A B 1992 *Phys. Fluids B* **4** 2441
- [46] Waelbroeck F L, Dong J Q, Horton W and Yushmanov P N 1994 *Phys. Plasmas* **1** 3742
- [47] Waltz R E, Kerbel G D and Milovich J 1994 *Phys. Plasmas* **1** 2229
- [48] Waltz R E, Staebler G M, Dorland W, Hammett G W, Kotschenreuther M and Konings J A 1997 *Phys. Plasmas* **4** 2482